

1 Kainate-type of glutamate receptors regulate development of glutamatergic
2 synaptic circuitry in the rodent amygdala

3 Maria Ryazantseva^{1,2}, Jonas Englund^{1,2}, Alexandra Shintyapina^{1,2}, Johanna Huupponen^{1,2}, Vasili
4 Shteinikov¹, Asla Pitkänen³, Juha M. Partanen¹, Sari E. Lauri^{1,2} *

- 5 1. Molecular and Integrative Biosciences Research Program, University of Helsinki, Finland
6 2. Neuroscience Center, University of Helsinki, Finland
7 3. A.I. Virtanen Institute for Molecular Sciences, University of Eastern Finland, Finland

8 * Lead contact and Corresponding author, e-mail sari.lauri@helsinki.fi

9

10

11 **Summary**

12 Perturbed information processing in the amygdala has been implicated in developmentally
13 originating neuropsychiatric disorders. However, little is known on the mechanisms that guide
14 formation and refinement of intrinsic connections between amygdaloid nuclei. We demonstrate
15 that in rodents the glutamatergic connection from basolateral to central amygdala (BLA-CeA)
16 develops rapidly during the first ten postnatal days, before external inputs underlying amygdala
17 dependent behaviors emerge. During this restricted period of synaptic development, kainate-type
18 of ionotropic glutamate receptors (KARs) are highly expressed in the BLA and tonically activated to
19 regulate glutamate release via a G-protein dependent mechanism. Genetic manipulation of this
20 endogenous KAR activity locally in the newborn LA perturbed development of glutamatergic input
21 to CeA, identifying KARs as a physiological mechanism regulating formation of the glutamatergic
22 circuitry in the amygdala.

23

24 *Keywords (<10)*

25 kainate receptor; glutamate receptor; amygdala; synaptic transmission; circuit development

26 **Introduction**

27 Kainate-type of ionotropic glutamate receptors (KARs) are expressed in different cell types in
28 various parts of the brain. While physiological roles for KARs in modulation of both glutamatergic
29 and GABAergic transmission have been described in the mature neural networks (Lerma &
30 Marquez, 2013), increasing evidence suggests predominant functions for KARs in the developing
31 circuitry. KARs modulate formation of glutamatergic contacts by regulating neurite growth
32 (Ibarretxe et al., 2007; Joseph et al., 2011; Marquez et al., 2013), filopodial dynamics (Chang and De
33 Camilli, 2001; Tashiro et al., 2006) and synaptic differentiation (Marchal and Mulle, 2004; Lanore et
34 al., 2012; Sakha et al. 2016). At immature hippocampal synapses, KARs control efficacy and short-
35 term dynamics of transmission by tonically regulating glutamate release probability (Lauri et al.,
36 2005; 2006). Interestingly, many of the developmental functions of KARs are mediated by non-
37 canonical G-protein dependent signaling mechanisms (Lauri et al., 2006; Tashiro et al., 2006;
38 Marquez et al 2013). In the absence of the early KAR activity, development of the glutamatergic
39 connectivity in the hippocampus is perturbed (Vesikansa et al., 2012; Lanore et al., 2012; Orav et al.,
40 2017). Thus, the existing data indicate KARs as key modulators of synaptic transmission and
41 plasticity during the critical window of synapse development in the hippocampus. However, the
42 applicability of these mechanisms to other areas of the developing brain remains largely unknown.

43 Amygdala represents another part of the limbic system involved in memory, emotion and
44 autonomic function. Basic architecture of the mammalian amygdala is present at birth, but similar
45 to hippocampus, it undergoes structural and functional change across extended developmental
46 period (Tottenham and Sheridan, 2010). External inputs to basolateral amygdala (BLA) develop
47 postnatally, the thalamic inputs being detectable in around P7 (Bouwmeester et al., 2002), while
48 cortical innervation emerge gradually between P10 – P21 (Arruda –Carvalho et al., 2017). Both
49 lateral (LA) and basal amygdala (BA) nuclei have strong glutamatergic projections to the central
50 amygdala (CeA), where the principal cells are GABAergic (Sah et al., 2003; Pape and Pare, 2010).
51 However, practically nothing is known on the development of the intrinsic connections in the
52 amygdala.

53
54 Here we show that KAR subunits GluK1,2 and 5 are strongly expressed in the amygdala during early
55 postnatal development, temporally coinciding with rapid development of functional glutamatergic
56 synapses. In the newborn BLA, KARs are physiologically activated to regulate glutamate release
57 probability via a G-protein dependent mechanisms. Knockdown or overexpression of GluK1
58 expression locally in the newborn LA perturbed development of glutamatergic input to CeA,
59 suggesting that endogenous KAR activity is critical for development of the LA-CeA connections.
60 Interestingly, it was recently shown that enhanced activity of KARs in the adult amygdala, generated
61 via GluK4 overexpression, leads to severe changes in the circuit excitability and amygdala
62 dependent behaviors (Arora et al., 2018). Together, these data thus identify tonic KAR activity as a
63 mechanism modulating behaviorally relevant synaptic circuitry in the amygdala.

64

65

Results

Kainate receptors are highly expressed in the BLA during the first postnatal week

Based on the existing literature, at least subunits GluK1, GluK2 and GluK5 are expressed in the adult rat BLA (Bettler et al., 1990; Li et al., 2001) where they have been implicated in regulation of synaptic transmission and plasticity (Li et al., 2001; Ko et al., 2005; Shin et al., 2010). To characterize the developmental profile for expression of various KAR subunits, BLA was dissected from acute rat brain slices at three developmental stages (postnatal day (P)4, P14, and P50). Absolute quantitative RT-PCR analysis of *Grik1-5* mRNAs, encoding for subunits GluK1-5, revealed that during early postnatal development (P4), the predominant KAR subunits in the BLA are *Grik1*, *Grik2* and *Grik5*, while *Grik3* and *Grik4* mRNAs were detected at low levels. During development, *Grik2* and *Grik5* mRNA expression remained relatively high (at P14 and P50, *Grik2*: $67 \pm 4\%$ and $69 \pm 10\%$ of the level at P4, respectively, ANOVA $F_{(2,21)}=4.0$, $p=0.034$; *Grik5*: $91 \pm 8\%$ and $163 \pm 15\%$, ANOVA $F_{(2,7)}=4.5$, $p=0.055$) while *Grik1* and *Grik4* mRNA levels were strongly downregulated already during the first two postnatal weeks (P14 and P50, *Grik1*: $32 \pm 5\%$ and $35 \pm 9\%$ of the level at P4, respectively, ANOVA $F_{(2,16)}=2.18$, $p < 0.001$; *Grik4*: $54 \pm 6\%$ and $42 \pm 5\%$, ANOVA on ranks $H_{(2)}=19.39$, $p < 0.001$). *Grik3* mRNA expression was undetectable at P14 and P50. Finally, the *Neto1* and *Neto2* mRNAs, encoding for KAR auxiliary subunits NETO1 and NETO2, were both detected in the neonatal BLA, *Neto2* representing the predominant subtype (Figure 1 A,B).

To verify KAR expression at protein level, Western blot was done from crude protein extracts from neonatal BLA using antibodies for GluK2/3 and GluK5. These antibodies have been previously validated using knockout tissue as a negative control (Ruiz et al., 2005; Wyeth et al., 2014). Unfortunately, selective specific antibodies for other KAR subunits are not available. Consistent with the qPCR data, GluK2/3 and GluK5 were clearly detected both at P4 and P14 BLA, at approximately the same levels (GluK2/3: ANOVA $F_{(1,4)}=5.48$, $p=0.079$; GluK5: ANOVA $F_{(1,4)}=2.72$, $p=0.174$; Figure 1 C).

KARs localize to both glutamatergic and GABAergic neurons in the neonatal amygdala

In situ hybridization (ISH) using fluorescent probes was used to study the pattern of KAR subunit expression in the amygdala in more detail. ISH signal in the various nuclei of the amygdala was analyzed in rat brain sections, cut from P4 and P14. In addition, sections from GAD67-GFP knock-in (*Gad1*^{+/GFP}) mice were analyzed to investigate the expression of various KAR subunits in GAD67GFP+ GABAergic neurons. In P4 *Gad1*^{+/GFP} sections, GFP expression was detected in $10.8 \pm 0.6\%$, $13.7 \pm 0.9\%$ and $99 \pm 0.4\%$ of DAPI stained cells in LA, BA and CeA, respectively.

At P4, mRNAs encoding subunits GluK1, GluK2 and GluK5 were detected in all the amygdala nuclei analyzed (LA, BA and CeA) (Figure 1D,E). *Grik1* mRNA was observed in both GAD67GFP positive (GABAergic) and negative (likely representing glutamatergic principal neurons) cells in the BLA ($25 \pm 5\%$ of GAD67GFP+ neurons at P4; Figure 1D). In the CeA, *Grik1* mRNA was detected in $30 \pm 2\%$ of the GAD67GFP positive neurons. Consistent with the qPCR data, *Grik1* mRNA was significantly downregulated in the amygdala nuclei during the first postnatal weeks (ISH signal at P14 as

percentage of P4, LA: $17 \pm 3\%$, ANOVA on ranks, $H_{(1)}=9.80$, $p<0.001$; BA: $38 \pm 6\%$, ANOVA $F_{(1,12)}=19.93$, $p<0.001$; CeA: $28 \pm 4\%$, ANOVA $F_{(1,12)}=60.87$, $p<0.001$; Figure 1E).

Grik2 mRNA was predominantly expressed in the GAD67GFP negative (glutamatergic) cells, and only detected in a minority of GABAergic neurons within the BLA ($18 \pm 3\%$ of GAD67GFP+ neurons at P4; Figure 1D). In the CeA, *Grik2* mRNA was detected in 42% of GAD67GFP+ neurons (Figure 1D). *Grik2* mRNA expression was slightly downregulated during development, although this effect reached statistical significance only in the LA (ISH signal at P14 as percentage of P4, LA: $71 \pm 10\%$, ANOVA, $F_{(1,10)}=14.7$, $p=0.003$; BA: $66 \pm 37\%$, ANOVA on ranks, $H_{(1)}=2.08$, $p=0.18$; CeA: $31 \pm 8\%$, ANOVA on ranks, $H_{(1)}=2.08$, $p=0.18$; Figure 1E).

Grik5 mRNA was detected in both GAD67GFP positive and negative cells ($30 \pm 2\%$ of GAD67GFP+ neurons at P4) in the BLA. *Grik5* mRNA was also strongly expressed in $43 \pm 6\%$ GAD67GFP+ neurons in the CeA at P4 (Figure 1D). At P14, the same overall pattern of staining remained, except for slight but not significant downregulation of *Grik5* expression level in the CeA (ISH signal at P14 as percentage of P4, LA: $103 \pm 15\%$, BA: $107 \pm 12\%$; CeA: $77 \pm 9\%$, ANOVA $F_{(1,10)}=2.06$, $p=0.18$; Figure 1E).

Early postnatal development of glutamatergic synaptic connectivity in the amygdala

The high developmental expression of KAR subunits in the amygdala is similar to that in the hippocampus, where KARs have specific developmentally restricted functions related to maturation of the glutamatergic synaptic connectivity. However, the exact time course for development of glutamatergic synaptic inputs to various nuclei in the amygdala is not known. Therefore, we recorded miniature excitatory postsynaptic currents (mEPSCs) from LA, BA and CeA neurons to get a general view on the functional glutamatergic inputs at different stages of postnatal development. The recorded cells were filled with biocytin for post-hoc analysis of the spine density.

Interestingly, the mean mEPSC frequency, reflecting the density of functional glutamatergic inputs to the recorded neuron, increased with a distinct developmental time course at different nuclei. In the LA and BA, the mEPSC frequency increased significantly from P4-7 to P9-11 (LA: $479 \pm 88\%$, ANOVA on ranks, $H_{(1)}=10.42$, $p=0.001$; BA: $493 \pm 95\%$, ANOVA on ranks, $H_{(1)}=10.38$, $p=0.001$), and from P9-11 to P14-16 (LA: $240 \pm 50\%$, ANOVA $F_{(1,15)}=6.69$, $p=0.021$; BA: $196 \pm 35\%$, ANOVA $F_{(1,16)}=4.60$, $p=0.048$), but reached a plateau at the second postnatal week (Figure 2 A,B). In contrast, in the CeA the mEPSC frequency increased rapidly between P4-7 and P9-11 ($353 \pm 62\%$, ANOVA on ranks, $H_{(1)}=7.78$, $p=0.005$), after which no significant changes in the mean frequency of the events were detected within the analyzed time window (Figure 2 A,B). The mEPSC amplitudes remained stable throughout the early postnatal development (not shown).

Spine maturation takes place later than formation of a functional synapse. Visualization of dendritic spines of the biocytin filled neurons revealed that the mean spine density stabilized earlier in the CeA as compared to BLA (spine density, % increase P14-16 vs P20-21, LA: $149 \pm 13\%$,

144 ANOVA $F_{(1,14)}=5.30$, $p=0.037$; BA: 166 ± 25 %, ANOVA $F_{(1,12)}=5.19$, $p=0.042$; CeA: 94 ± 7 %, ANOVA
145 $F_{(1,14)}=0.149$, $p=0.71$; Figure 2 C,D). This is consistent with the idea that the glutamatergic synapses
146 to CeA form rapidly during the first two postnatal weeks in rats, while the inputs to BLA develop
147 with an extended time course.

148 *Ionotropic KAR function is not detected in the BLA during the first postnatal week*

149 The developmental peak in KAR, and particularly GluK1 expression was associated with the time of
150 rapid development of glutamatergic synapses in the BLA and CeA. To understand the physiological
151 roles of KARs in the developing circuit, we mapped functional ionotropic KARs in the neonatal
152 amygdala using agonist application during voltage clamp recordings. Surprisingly, application of
153 kainate (KA, 2 μ M) in the presence of selective antagonists for AMPA, NMDA and GABA receptors
154 (2 μ M NBQX, 50 μ M APV and 100 μ M PiTX, respectively) induced no or only a very small current
155 (LA: 6 ± 1 pA; BA: 8 ± 1 pA) in the BLA neurons during the first postnatal week (P4-P7), while a
156 marked inward current was observed later on in development (P14-P16) (LA: 81 ± 19 pA, BA 37 ± 5
157 pA) (Figure 3 A,B). In the CeA, a small KA induced inward current was detected already at P4-P6
158 (15 ± 2 pA), but the current was significantly larger at P14-16 (27 ± 3 pA, ANOVA on ranks,
159 $H_{(1)}=8.00$, $p=0.005$)(Figure 3 A,B). Since kainate might cause rapid desensitization of the receptors,
160 we also used another KAR agonist, domoate to confirm the result in the first postnatal week (P4-
161 P7). Application of domoate (500 nM) induced no current in LA neurons (4 ± 1 pA), but in BA a
162 small inward current was detected (17 ± 1 pA; Figure 3 C,D). Thus, the high expression of the KAR
163 subunits in the newborn LA does not correlate with ionotropic function of KARs, which emerges
164 after the second postnatal week. Small KAR-dependent currents were detected in BA and in
165 particular, in the CeA already at P4-P6, but contrast to the declining mRNA expression profile, the
166 ionotropic function increased towards the second postnatal week.

167

168 *KARs regulate glutamatergic inputs to BA and CeA during the first postnatal week*

169 At immature CA3-CA1 synapses, presynaptic GluK1 subunit containing KARs tonically regulate
170 glutamate release probability in a G-protein and PKC-dependent manner (Lauri et al., 2006; Sallert
171 et al., 2007). To test whether KARs might have similar functions in the newborn amygdala, we
172 studied the effect of 200 nM ACET, a selective antagonist for GluK1 subunit containing KARs
173 (Dargan et al., 2009), on mEPSCs in LA, BA and CeA during first (P4-7) and second postnatal weeks
174 (P10-16). In LA, ACET had no significant effect on mEPSCs at P4-6 (frequency 92 ± 14 % of control,
175 paired t-test $t_{(6)}=-0.80$, $p=0.45$, amplitude 101 ± 8 % of control) or at P14-P16 (frequency 91 ± 3 %,
176 paired t-test $t_{(5)}=2.56$, $p=0.051$; amplitude 103 ± 4 % of control; Figure 4A). In contrast, ACET
177 application resulted in a small but significant increase in the mEPSC frequency in BA at P4-P6 (130
178 ± 4 % of control, signed rank test, $Z=2.93$, $p=0.004$), but not at P14-P16 (92 ± 7 %, paired t-test,
179 $t_{(3)}=1.11$, $p=0.35$) (Figure 4B). ACET had no effect on mEPSC amplitude at either developmental
180 time point (97 ± 1 % and 100 ± 4 % of control, respectively). The developmentally restricted effect
181 of GluK1 KAR antagonism on mEPSC frequency in BA is similar to that previously characterized in

182 the area CA1 of hippocampus (Lauri et al., 2006), indicative of tonic KAR mediated inhibition of
183 glutamate release.

184 In CeA, ACET application resulted in a marked depression of mEPSC frequency in first postnatal
185 week (P5-6) ($73 \pm 5 \%$, paired t-test, $t_{(10)}=4.22$, $p=0.0018$) without affecting their amplitude (99 ± 3
186 $\%$). Also this effect was developmentally restricted, as ACET had no effect of mEPSCs at P10-P11
187 CeA (frequency $101 \pm 7 \%$, amplitude $98 \pm 4 \%$; Figure 4C).

188 These data show that GluK1 subunit containing KARs are physiologically activated to regulate
189 glutamatergic transmission in the amygdala during the first postnatal week. Their effect is area
190 and/or cell type specific, with KAR mediated inhibition and facilitation of transmission at
191 glutamatergic inputs to BA and CeA, respectively.

192

193 *Transmission at immature BLA – CeA synapses is tonically facilitated by presynaptic G-protein*
194 *coupled KARs*

195 The data on KAR expression and function at the neonatal amygdala so far show 1) high expression
196 of GluK1, GluK2 and GluK5 in the BLA 2) low ionotropic KAR activity in the BLA and 3) KAR
197 dependent regulation of mEPSC frequency in the BA and CeA. One interpretation of these data is
198 that GluK1 subunit containing KARs, expressed in the principal cells of LA (and BA), are targeted to
199 axons to regulate transmitter release at emerging projections to BA and CeA via a mechanism that
200 does not require ionotropic activity.

201 To investigate this we focused to study the pathway from BLA to CeA at P5-6, and recorded EPSCs
202 from CeA in response to electrical stimulation of the LA. Consistent with hypothesis that
203 presynaptic GluK1 subunit containing KARs regulate transmission at this pathway, ACET
204 application resulted in significant reversible depression of the EPSC amplitude ($62 \pm 5 \%$ of control,
205 paired t-test, $t_{(7)}=-3.586$, $p=0.009$) that was associated with an increase in paired – pulse ratio
206 (PPR) ($150 \pm 14 \%$, paired t-test, $t_{(8)}=4.01$, $p=0.0039$) (Figure 5A). Furthermore, EPSCs evoked by
207 single pulse or paired pulses with 50 ms interval of BLA stimulation were completely blocked by
208 the AMPA-receptor selective antagonist GYKI53655 ($25 \mu\text{M}$) ($8 \pm 2 \%$ of control, paired t-test, $t_{(7)}=-$
209 3.679 , $p=0.008$), excluding the possibility that postsynaptic KARs significantly contributed to the
210 eEPSC in this pathway (Figure 5B). Adult CeA neurons also receive glutamatergic input from extra-
211 amygdalar brain regions, including sensory input from the auditory cortex and thalamus (Keifer et
212 al., 2015). However, during the first postnatal week, we could not observe any postsynaptic
213 responses in CeA neurons to stimulation of external and internal capsules, the regions containing
214 cortical and thalamic projections to amygdala (not shown). This suggests that external inputs to
215 CeA are not present during the first postnatal week and thus do not contribute to the observed
216 changes in mEPSC frequency in response to KAR antagonism in the neonate (P5-6) CeA.

217

218 Pharmacological tools were used to further characterize the mechanism involved. Application of a
219 broad KAR agonist KA (500 nM) and ATPA ($1 \mu\text{M}$), agonist selective for GluK1 subunit containing

220 KARs, resulted in transient increase in mEPSC frequency in P5-P6 CeA (KA: 146 ± 27 %, paired t-
221 test, $t_{(6)}=4.24$, $p=0.0055$; ATPA: 191 ± 21 %, paired t-test $t_{(6)}=3.14$, $p=0.02$; Figure 5C,D), with no
222 effect on mEPSC amplitude (91 ± 8.8 % for KA and 100 ± 13 % for ATPA). The peak increase in
223 mEPSC frequency in response to ATPA and KA was comparable in size or if anything, slightly larger
224 in ATPA as compared to KA (ANOVA, $F_{(1,12)}=4.50$, $p=0.055$), suggesting that GluK1 subunit
225 containing receptors can fully account for KAR regulation of transmission at this synapse without
226 additional (GluK1 lacking) KAR populations involved.

227

228 Finally, ACET had no effect on mEPSCs in P4-P6 CeA in slices that were preincubated in presence of
229 pertussis toxin (PTX), a selective inhibitor of the $G\alpha i/o$ signalling (mEPSC frequency in ACET, $108 \pm$
230 17 % of control; paired t-test $t_{(4)}=1.243$, $p=0.282$; Figure 5E). The incubation procedure itself had
231 no effect on the regulation of transmission by KARs, as ACET application resulted in significant
232 depression of mEPSC frequency in slices incubated under control conditions (72 ± 12 %, paired t-
233 test, $t_{(4)}=2.934$, $p=0.043$). Together, these data indicate that GluK1-subunit containing KARs
234 upregulate glutamate release at immature BLA-CeA synapses via a G-protein coupled signalling
235 mechanism.

236

237 *Loss of GluK1 in the amygdala in a cKO mouse model impairs glutamatergic innervation and* 238 *maturation of CeLA neurons*

239

240 Immature-type KAR activity is proposed to be critical for development and fine-tuning of the
241 glutamatergic synapses (Vesikansa et al., 2007; 2012; Orav et al., 2017). To investigate the
242 significance of the early KAR activity on the development and maturation of glutamatergic
243 transmission in the amygdala, we focused on studying the LA-CeA connections. To this end, we
244 generated a conditional (floxed) mouse model for *Grik1* (*Grik1* cKO), which allowed us to
245 inactivate GluK1 expression selectively in the neonate BLA *in vivo* with local injection of GFP-CRE
246 encoding AAV virus at P2-P4. The viral transduction covered 79 ± 5 % and 61 ± 8 % of cells in LA
247 and BA, respectively, and 10 ± 4 % of cells in the CeA, based on green fluorescence signal in DAPI
248 labeled cells at P21 (Figure 6A).

249

250 The consequences of targeted GluK1 knockout on glutamatergic synapses were studied with patch
251 clamp recordings of mEPSCs from acute slices at P21, followed by *post hoc* morphological analysis
252 of the recorded biocytin filled neurons. The recordings were made from GFP-CRE expressing
253 (GluK1 KO) and GFP expressing (control) neurons in the LA as well as from their target neurons in
254 the centrolateral (CeLA) part of the CeA, which, in contrast to <P16, can be clearly visualized at this
255 developmental stage in acute slices.

256

257 Loss of GluK1 had little or no effect on glutamatergic inputs to LA neurons, since there was no
258 significant difference in the mEPSC frequency or amplitude between GFP-CRE and GFP- expressing
259 neurons (frequency 100 ± 9 % of GFP control, ANOVA $F_{(1,23)}=0.0004$, $p=0.99$; amplitude 96 ± 3 % of
260 GFP control, ANOVA $F_{(1,23)}=0.21$, $p=0.65$; Figure 6B). In contrast, in CeLA neurons, both mEPSC
261 frequency and amplitude were significantly lower in GFP-CRE slices as compared to controls

(frequency 38 ± 6 % of GFP control, ANOVA on ranks, $H_{(1)}=7.752$, $p=0.005$; amplitude 73 ± 6 % of GFP control, ANOVA $F_{(1,19)}=10.226$, $p=0.005$; Figure 6B). *Post hoc* morphological analysis indicated that the loss of mEPSCs in the CeLA neurons was associated with a significant reduction in the spine density (61 ± 12 % of GFP control, ANOVA $F_{(1,22)}=10.19$, $p=0.004$; Figure 6C) and interestingly, lower dendritic length (54 ± 7 % of GFP control, ANOVA $F_{(1,19)}=10.41$, $p=0.004$; Figure 6D) and branching (two-way ANOVA, $F_{(19,418)}=2.89$, $p<0.0001$; Figure 6D). No differences in dendritic morphology were observed between GFP-CRE and GFP expressing neurons in the LA (Figure 6 – figure supplement 2).

These data pinpoint GluK1 in maturation of CeLA but not LA neurons. Following GluK1 knockout, the spine density and dendritic morphology in CeLA neurons was comparable to those at P10 in wildtypes (Figure 6 – figure supplement 3), suggesting that absence of GluK1 disrupted developmental maturation of the dendritic tree in CeLA neurons. Consistent with this idea, inactivation of GluK1 expression in BLA at a later developmental stage (BLA virus injection P14, *ex vivo* recording at P35) had no effect on mEPSCs (mEPSC frequency: 111 ± 10 % of control, ANOVA $F_{(1,15)}=0.411$, $p=0.531$; amplitude: 106 ± 7 % of control, ANOVA on ranks, $H_{(1)}=0.454$, $p=0.50$; Figure 6E), spine density (90 ± 8 % of control, ANOVA $F_{(1,17)}=0.452$, $p=0.51$; Figure 6F), dendritic length (107 ± 8 % of control, ANOVA $F_{(1,16)}=0.283$, $p=0.602$; Figure 6G) or dendritic intersections (two-way ANOVA $F_{(15,195)}=0.7235$, $p=0.76$, Figure 6G) in CeLA neurons.

Loss of GluK1 in the amygdala perturbs glutamatergic synaptic transmission and network excitability at the LA- CeLA circuitry

To understand the consequences of targeted GluK1 knockout on glutamatergic projections from LA to CeLA in more detail, we studied the properties of synaptic transmission using evoked responses. Specifically, we investigated the input/output relationship, AMPA/NMDA ratio and paired pulse ratio (PPR) of EPSCs, recorded from CeLA in response to LA stimulation in slices from *Grik1* cKO mice (P21) that were injected with GFP and GFP-CRE encoding AAV viruses in BLA at P2-4. The stimulus-response relationship of EPSCs, evoked by LA stimulation using fixed intensities, was steeper in control (GFP) slices as compared GFP-CRE group (two-way ANOVA, $F_{(16, 48)}=4.54$, $p<0.0001$; Figure 7A). In addition, the AMPA/NMDA ratio was significantly lower in the GFP-CRE slices as compared to controls (39 ± 8 % of control, ANOVA on ranks, $H_{(1)}=4.973$, $p=0.026$; Figure 7B). There was no difference in the paired pulse ratio (105 ± 18 % of control, ANOVA $F_{(1,18)}=0.0572$, $p=0.814$; Figure 7C). Thus, loss of GluK1 in the BLA is associated with significantly weaker AMPA-R mediated synaptic transmission from LA to CeLA.

Finally, the significance of targeted GluK1 knockout on amygdala excitability was assessed by recording spontaneous EPSCs and IPSCs from CeLA. Regular firing (RF) and late firing (LF) neuron populations were analysed separately given the recent data suggesting that overexpression of KARs has dissimilar effects on glutamatergic inputs to these neurons (Arora et al., 2017). We found that developmental loss of GluK1 specifically affected glutamatergic inputs to the LF cell population, where sEPSC frequency was significantly lower in the GFP-CRE slices as compared to

304 GFP controls (sEPSC frequency, 56 ± 5 %, ANOVA $F_{(1,22)}=5.54$, $p=0.028$; Figure 7D). There was no
305 significant difference in the sEPSCs between the groups in the RF cells (GFP-CRE, 95 ± 14 % of
306 control, ANOVA on ranks, $H_{(1)}=1.76$, $p=0.184$). sIPSC frequency was slightly but not significantly
307 higher in RF neurons in GFP-CRE slices as compared to controls (LF: 115 ± 25 %; ANOVA on ranks,
308 $H_{(1)}=0.97$, $p=0.33$; RF: 173 ± 32 %, ANOVA on ranks, $H_{(1)}=3.21$, $p=0.073$; Figure 7D).

309

310 These data indicate that loss of GluK1 weakens glutamatergic projections from LA to CeLA, leading
311 to significant changes in the excitation-inhibition balance in the amygdala circuit. Specifically,
312 GluK1 deficiency was associated with a significantly lower E/I ratio in the late firing neurons in the
313 CeLA (sEPSC/sIPSC ratio in GFP-CRE and GFP groups, LF neurons: 9.9 ± 2 and 4.4 ± 0.6 , ANOVA on
314 ranks, $H_{(1)}=4.91$, $p=0.027$; RF neurons: 6.3 ± 2.4 and 4.8 ± 1.7 , ANOVA on ranks, $H_{(1)}=0.48$,
315 $p=0.488$).

316

317 *Presynaptic GluK1 KARs guide development of glutamatergic synaptic input to the CeA*

318

319 To confirm that the observed effects at CeLA neurons were indeed due to the early endogenous
320 activity of GluK1 in the LA, we used lentiviral vectors to manipulate GluK1 expression in neonatal
321 rats. Lentiviral shRNA and overexpression produce faster changes in gene expression as compared
322 to AAV – CRE mediated inactivation of a floxed allele, allowing the consequences of P1-4 injection
323 to be analysed already at P10-11. In addition, the injected lentiviruses produced a transduction
324 that was spatially restricted to LA (GFP expression as a percentage of all DAPI positive cells, LA: 59
325 ± 5 % , BA: 0.7 ± 0.4 %, CeA: 0.1 ± 0.4 %; Figure 8A), thus selectively targeting the presynaptic
326 /axonal GluK1 receptors in the LA-CeA projections.

327 In slices with local lentiviral expression of *Grik1* shRNA in the LA, mEPSC frequency in CeA at P10-
328 P11 was significantly lower as compared to controls expressing a mock shRNA construct (38 ± 18
329 %, ANOVA, $F_{(1,9)}=7.59$, $p=0.02$; Figure 8B). Accordingly, GluK1 overexpression (oe) in the LA was
330 associated with significantly higher mEPSC frequency in the CeA as compared to GFP expressing
331 controls at P14 (188 ± 38 %, ANOVA on ranks, $H_{(1)}=4.77$, $p=0.029$; Figure 8C). Neither, *Grik1* shRNA
332 or GluK1 oe had a significant effect on mEPSC amplitude (71 ± 12 %, ANOVA $F_{(1,9)}=3.31$, $p=0.106$;
333 and 91 ± 11 %, ANOVA $F_{(1,19)}=0.45$, $p=0.51$, respectively). Importantly, GluK1 oe in the LA
334 recapitulated the tonic KAR dependent regulation of mEPSC frequency in the CeA at a
335 developmental stage (P14) when this regulation was no longer observed at control or GFP
336 expressing slices. Thus, in slices with LA-specific GluK1 oe, ACET application resulted in a significant
337 decrease in the mEPSC frequency in CeA cells (73 ± 11 % of control, paired t-test, $t_{(4)}=5.496$,
338 $p=0.0053$), but had no effect in control (GFP expressing) slices (103 ± 7 % of control, paired t-test
339 $t_{(4)}=1.267$, $p=0.274$) (Figure 8D). These results confirm that presynaptic GluK1 KARs, located in the
340 axons of LA principal neurons, regulate glutamatergic transmission to CeA.

341 The ongoing GluK1 dependent facilitation of transmission contributes to the observed increase in
342 the basal mEPSC frequency in GluK1 oe slices. In addition, morphological analysis of the CeA
343 neurons indicated that the number of dendritic intersections in both apical and distal dendrites
344 was significantly higher in GluK1 oe slices as compared to controls (total dendritic length in GluK1

oe slices, 200 ± 22 % of GFP, ANOVA $F_{(1,11)}=22.6$, $p<0.001$; dendritic intersections, two-way ANOVA $F_{(8, 90)}= 3.014$, $p=0.0049$; Figure 8E). In contrast, no significant differences in the density of dendritic spines were detected (mean density of spines in GluK1 oe slices, 116 ± 7 % of GFP control; ANOVA $F_{(1,14)}=1.48$, $p=0.24$; Figure 8F).

Together, these data indicate that developmental manipulation of GluK1 expression in the LA results in lasting changes in glutamatergic synaptic transmission from LA to CeA and support that presynaptic GluK1 subunit containing KARs are required for appropriate development of intrinsic glutamatergic connections in the amygdala.

353

354 **Discussion**

Given the importance of the amygdala in several developmentally originating neuropsychiatric disorders, it is surprising how little is understood on the mechanisms that govern formation and refinement of the synaptic circuitry in the amygdala. In particular, very little is known on the development of the projections from the BLA to CeA, critical elements in the neural circuits mediating fear and anxiety (Duvarci and Pare 2014; Herry and Johansen 2014). Here we show that functional glutamatergic connections to CeA develop rapidly during the first 10-11 postnatal days in rats, before the external cortical inputs to amygdala emerge (Bouwmeester et al. 2002; Arruda Carvalho et al., 2017). Further, we demonstrate that during the time of intense synaptogenesis, transmission to CeA is strongly regulated by physiological activity of presynaptic KARs, which is critical for appropriate development of the LA-CeA synapses.

Histological and functional evidence indicate that maturation of the intrinsic and extrinsic connectivity in the rodent BLA occurs postnatally, being completed around P21-P28 (Nair & Gonzalez-Lima 1999; Morys et al., 1998; Bosch and Ehrlich 2015; Ryan et al., 2016; Arruda – Carvalho et al., 2017), in parallel with emergence of amygdala – dependent forms of associative emotional learning (e.g. Landers & Sullivan 2012; Hartley and Lee 2015; Deal et al., 2016). Consistently, we found that spine density at BLA neurons increased gradually during the first three postnatal weeks while the density of functional inputs, assessed by mEPSC frequency, stabilized after the second postnatal week. Interestingly, glutamatergic inputs to the CeA reached maturity earlier as compared to BLA, the mEPSC frequency stabilizing already at P10-11 and spine density at around P14-16. Based on tracing studies, the external inputs to amygdala develop gradually from P7 onwards, most cortical inputs arriving only after the second postnatal week (Bouwmeester et al. 2002; Arruda Carvalho et al., 2017). However, CeA receives strong glutamatergic input from BLA (Pape and Pare, 2010; Sah et al., 2003), suggesting that rapid increase in mEPSC frequency between P5-P10 reflects mainly formation of the intrinsic amygdala circuits and specifically, development of the BLA – CeA connectivity. These data support that the local circuit in the amygdala is wired before the cortical inputs underlying behavior actuate.

Kainate receptors are highly expressed in the adult amygdala (Bettler et al., 1990; Li et al., 2001). However, no previous data on the expression and function of KARs during amygdala development

exists. Our data show that the low-affinity subunits GluK1 and GluK2 and the high-affinity subunit GluK5 are strongly expressed in the BLA during the first postnatal week, when the glutamatergic synapses are rapidly developing. Early in development, all the subunits were also detected in the central amygdala. The expression pattern of various KAR subunits in the newborn amygdala showed no evident cell-type specificity, thus giving little insight into their functions in the neonatal BLA circuitry. Yet, the finding that GluK1 expression was strongly downregulated during development, in parallel with maturation of synaptic connectivity, is reminiscent to hippocampus where this subunit has central role in regulating synaptic plasticity and formation of CA3-CA1 synaptic connections (Lauri et al., 2006; Vesikansa et al., 2012; Clarke et al., 2014; Orav et al., 2017).

Intriguingly, during the first postnatal week corresponding to the developmental peak in expression of most KAR subunits, ionotropic activity of KARs was weak in the BLA. Contrary to the declining mRNA expression profile, KAR mediated inward currents were significantly increased during development in all amygdala nuclei studied. Instead, we found that tonic G-protein coupled signaling via GluK1 subunit containing KARs regulated glutamate release in a developmentally restricted manner. Our data thus supports that G-protein coupled 'non-canonical' signaling is a predominant mode of KAR activity during the time of intense synaptogenesis, while the emergence of ionotropic KARs correlates with circuit maturation (Marchal and Mulle, 2004).

In adult BLA, KAR activity facilitates glutamate release (e.g. Arodianou-Anderjaska et al., 2012; Arora et al., 2018) indicating that presynaptic KARs are present in adult but are functionally distinct from the immature-type GluK1 subunit containing receptors that tonically inhibit glutamate release in the BA. In the CeA, tonic KAR dependent facilitation of glutamate release was detected during the first postnatal week of life. According to our results, presynaptic KARs are not endogenously active in the juvenile (P14-16) amygdala; however, previous studies using KAR antagonists with a broader subunit specificity (UBP302, UBP310) have detected endogenous KAR activity also in the adult BLA (Arodianou-Anderjaska et al., 2012; Arora et al., 2018). During first weeks of life, concentration of ambient glutamate is high (e.g. Hanson et al., 2019) and sufficient to activate high-affinity GluK1 subunit containing KARs (Lauri et al., 2006; Segerstråle et al., 2010). The developmental increase in glial glutamate uptake thus provides a plausible mechanism for the decline in the tonic KAR activity. Parallel changes in KAR subunit composition affecting subcellular localization and affinity of the receptors (e.g. Vesikansa et al., 2012) likely contribute to the switch from immature to adult type KAR activity. The previous findings showing coupling of GluK1 to G-proteins (Rutkowska-Włodarczyk et al., 2015) and recapitulation of immature-type synaptic signaling by GluK1c overexpression (Vesikansa et al., 2012; present data) support the view that expression of GluK1 and in particular, the GluK1c splice variant, is central to the early metabotropic KAR activity. In addition, the high agonist affinity, permitting the tonic activation, depends on availability of subunits GluK4/5 as well as the auxiliary subunits NETO1/2 (reviewed by Lerma and Marquez, 2013).

Recently, it was demonstrated that overexpression of KAR subunit GluK4 enhances tonic KAR activity in the adult amygdala and leads to profound changes in the circuit excitability (Arora et al.,

2018). Since the immature-type tonic KAR activity temporally coincided with rapid development of functional glutamatergic synapses in the amygdala, we presumed that the physiological role of this activity is to modulate development of the amygdala circuitry. Consistently, local GluK1 knockdown in the LA during the time of rapid development of the BLA-CeA connectivity, but not later on in life, resulted in significantly impaired glutamatergic transmission from LA to CeA. Loss of GluK1 expression had no effect on glutamatergic inputs to the LA neurons themselves, which supports the idea that circuit development is predominantly modulated by presynaptic / axonal GluK1 KARs at the LA-CeLA projections.

Weakening of glutamatergic transmission at the LA-CeLA projections following GluK1 inactivation was associated with changes in dendritic morphology in the CeLA target neurons, involving reduction in both, the spine density as well as size of the dendritic tree. Likewise, prolonging the developmental KAR activity via GluK1 overexpression resulted in an expansion of the dendritic tree of CeA neurons, consistent with the idea that KAR activity promotes both functional and morphological maturation of the amygdala neuronal networks. The changes in dendritic morphology likely contribute to the observed changes in glutamatergic drive. However, our data does not indicate whether presynaptic KARs directly influence dendritic development of the CeA neurons via some transsynaptic signaling pathway or whether the morphological alterations resulted secondarily from the KAR dependent changes in glutamatergic transmission early in life.

The endogenous KAR activity particularly affected glutamatergic inputs to the subpopulation of late firing neurons in the CeLA, which displayed significantly lower frequency of sEPSCs in preparations where GluK1 activity was knocked out. Since there were no parallel changes in PPR of evoked responses, loss of ongoing KAR dependent regulation of neurotransmitter release is unlikely to explain the functional phenotype in GluK1 deficient amygdala in juvenile/adult stage. Rather, all the available data supports the view that loss of glutamatergic input to the LF neurons is a result of perturbed development of glutamatergic synapses in the absence of GluK1. Excitability of the LF (PKC- δ +) neurons in the CeA controls anxiety-like behaviors in mice (Tye et al., 2011; Cai et al., 2014) suggesting that impaired early KAR activity, leading to altered excitatory drive to LF CeA neurons, might be a causative factor in developmentally originating anxiety disorders.

In summary, we have here characterized a physiological KAR mechanism regulating formation of the glutamatergic synaptic circuitry in the amygdala. The endogenous KAR signaling operates during the time of intense synaptogenesis, before the onset of amygdala-dependent behaviors and emergence of the cortical inputs. KARs have been implicated in CNS disorders related to dysfunction of the limbic areas, including mood and anxiety disorders, autism, schizophrenia, as well as epilepsy and stroke (Lerma & Marquez, 2013; Jane et al., 2009). Indeed, KAR dependent modulation of the transmission from BLA to CeA is associated with aberrant amygdala dependent behaviors in adult mice, resembling the human endophenotypes associated with autism and schizophrenia (Arora et al., 2018). Our data indicate that the KAR-dependent circuit remodeling physiologically operates in the developing brain, and support the idea that KAR malfunction during circuit development might predispose to neurological disorders later on in life.

464 ***Acknowledgements***

465 We thank Prof. Andreas Lüthi and his group members for their expert help with amygdala slice
466 electrophysiology. Kirsi Kolehmainen, Erja Huttu and Outi Kostia are acknowledged for the
467 outstanding technical help. This study was financially supported by the Academy of Finland, Sigrid
468 Juselius Foundation and Jane and Aatos Erkkö foundation.

469
470 ***Declaration of interests***

471 The authors declare no competing interests.

472 **References**

- 473 Aroniadou-Anderjaska, V., Pidoplichko, V.I., Figueiredo, T.H., Almeida-Suhett, C.P., Prager, E.M., Braga, M.F.
474 (2012). Presynaptic facilitation of glutamate release in the basolateral amygdala: a mechanism for the
475 anxiogenic and seizurogenic function of GluK1 receptors. *Neuroscience* 221, 157-69.
- 476 Arora, V., Pecoraro, V., Aller, M.I., Román, C., Paternain, A.V., and Lerma, J. (2018). Increased Grik4 Gene
477 Dosage Causes Imbalanced Circuit Output and Human Disease-Related Behaviors. *Cell Rep.* 23, 3827-3838.
- 478 Arruda-Carvalho, M., Wu, W.C., Cummings, K.A., and Clem, R.L. (2017). Optogenetic Examination of
479 Prefrontal-Amygdala Synaptic Development. *J Neurosci.* 37, 2976-2985.
- 480 Berdel, B., Morys, J., and Maciejewska, B. (1997). Neuronal changes in the basolateral complex during
481 development of the rat's amygdala. *Int. J. Dev. Neurosci.* 15, 755–765.
- 482 Bettler, B., Boulter, J., Hermans-Borgmeyer, I., O'Shea-Greenfield, A., Deneris, E.S., Moll, C., Borgmeyer, U.,
483 Hollmann, M., and Heinemann, S. (1990). Cloning of a novel glutamatereceptor subunit, GluR5: expression
484 in the nervous system during development. *Neuron* 5, 583–595.
- 485 Bosch, D., and Ehrlich, I. (2015). Postnatal maturation of GABAergic modulation of sensory inputs onto
486 lateral amygdala principal neurons. *J Physiol.* 593, 4387-409.
- 487 Bouwmeester, H., Smits, K., and Van Ree, J.M. (2002). Neonatal development of projections to the
488 basolateral amygdala from prefrontal and thalamic structures in rat. *J Comp Neurol* 450, 241–255.
- 489 Cai, H., Haubensak, W., Anthony, T.E., Anderson, D.J. (2014) Central amygdala PKC- δ + neurons mediate the
490 influence of multiple anorexigenic signals. *Nature Neurosci* 17, 1240–1248.
- 491 Chang, S., and De Camilli, P. (2001). Glutamate regulates actin-based motility in axonal filopodia. *Nat*
492 *Neurosci.* 4, 787-93.
- 493 Clarke, V.R., Molchanova, S.M., Hirvonen, T., Taira, T., and Lauri, S.E. (2014). Activity-dependent
494 upregulation of presynaptic kainate receptors at immature CA3-CA1 synapses. *J Neurosci.* 34, 16902-16.
- 495 Dargan, S.L., Clarke, V.R., Alushin, G.M., Sherwood, J.L., Nisticò, R., Bortolotto, Z.A., Ogden, A.M., Bleakman,
496 D., Doherty, A.J., Lodge, D., Mayer, M.L., et al. (2009). ACET is a highly potent and specific kainate receptor
497 antagonist: Characterisation and effects on hippocampal mossy fibre function. *Neuropharmacology* 56,
498 121-30.
- 499 Deal, A.L., Erickson, K.J., Shiers, S.I., and Burman, M.A. (2016). Limbic system development underlies the
500 emergence of classical fear conditioning during the third and fourth weeks of life in the rat. *Behav Neurosci.*
501 130, 212-30.
- 502 Donato, F., Rompani, S.B., and Caroni, P. (2013). Parvalbumin-expressing basket-cell network plasticity
503 induced by experience regulates adult learning. *Nature* 504, 272-6.
- 504 Duvarci, S., and Pare, D. (2014). Amygdala microcircuits controlling learned fear. *Neuron* 82, 966–980.
- 505 Foehring, R.C., and Scroggs, R.S. (1994). Multiple high-threshold calcium currents in acutely isolated rat
506 amygdaloid pyramidal cells. *J Neurophysiol.* 71, 433-6.
- 507 Hanson, E., Armbruster, M., Lau, L.A., Sommer, M.E., Klaft, Z.J., Swanger, S.A., Traynelis, S.F., Moss, S.J.,
508 Noubary, F., Chadchankar, J., Dulla, C.G. (2019). Tonic Activation of GluN2C/GluN2D-Containing NMDA
509 Receptors by Ambient Glutamate Facilitates Cortical Interneuron Maturation. *J Neurosci.* 39(19), 3611-
510 3626.

511 Hartley, C.A., and Lee, F.S. (2015). Sensitive periods in affective development: nonlinear maturation of fear
512 learning. *Neuropsychopharmacology* 40, 50-60.

513 Herry, C., and Johansen, J.P. (2014). Encoding of fear learning and memory in distributed neuronal circuits.
514 *Nat Neurosci.* 17, 1644-54.

515 Ibarretxe, G., Perrais, D., Jaskolski, F., Vimeney, A., and Mulle, C. (2007). Fast regulation of axonal growth
516 cone motility by electrical activity. *J Neurosci* 27, 7684-95.

517 Jane, D.E., Lodge, D., and Collingridge, G.L. (2009). Kainate receptors: pharmacology, function and
518 therapeutic potential. *Neuropharmacology* 56, 90-113.

519 Joseph, D.J., Williams, D.J., and MacDermott, A.B. (2011) Modulation of neurite outgrowth by activation of
520 calcium-permeable kainite receptors expressed by rat nociceptive-like dorsal root ganglion neurons. *Dev*
521 *Neurobiol* 71, 818–835.

522 Keifer, O.P. Jr., Hurt, R.C., Ressler, K.J., Marvar, P.J. (2015) The Physiology of Fear: Reconceptualizing the
523 Role of the Central Amygdala in Fear Learning. *Physiology (Bethesda)* 30(5), 389-401.

524 Ko, S., Zhao, M.G., Toyoda, H., Qiu, C.S., and Zhuo, M. (2005). Altered behavioral responses to noxious
525 stimuli and fear in glutamate receptor 5 (GluR5)- or GluR6-deficient mice. *J Neurosci.* 25, 977-84.

526 Landers, M.S., and Sullivan, R.M. (2012). The development and neurobiology of infant attachment and fear.
527 *Dev Neurosci* 34, 101–114.

528 Lanore, F., Labrousse, V.F., Szabo, Z., Normand, E., Blanchet, C., and Mulle, C. (2012). Deficits in
529 morphofunctional maturation of hippocampal mossy fiber synapses in a mouse model of intellectual
530 disability. *J Neurosci* 32, 17882-93.

531 Lauri, S.E., Vesikansa, A., Segerstråle, M., Maingret, F., Mulle, C., Collingridge, G., Isaac, J. and Taira, T.
532 (2006). Functional maturation of CA1 synapses involves activity-dependent loss of tonic kainate receptor-
533 mediated inhibition of glutamate release. *Neuron* 50, 415-29.

534 Lauri, S.E., Segerstråle, M., Vesikansa, A., Maingret, F., Mulle, C., Collingridge, G.L., Isaac, J.T., and Taira, T.
535 (2005). Endogenous activation of kainate receptors regulates glutamate release and network activity in the
536 developing hippocampus. *J Neurosci* 25, 4473-84.

537 Lerma, J., and Marques, J.M. (2013). Kainate receptors in health and disease. *Neuron* 80, 292-311.

538 Li, H., Chen, A., Xing, G., Wei, M.L., and Rogawski, M.A. (2001). Kainate receptor-mediated heterosynaptic
539 facilitation in the amygdala. *Nat Neurosci.* 4, 612-20.

540 Li, H., Penzo, M.A., Taniguchi, H., Kopec, C.D., Huang, Z.J., and Li B. (2013). Experience-dependent
541 modification of a central amygdala fear circuit. *Nat. Neurosci.* 16, 332–339.

542 Marchal, C., and Mulle, C. (2004). Postnatal maturation of mossy fibre excitatory transmission in mouse
543 CA3 pyramidal cells: a potential role for kainate receptors. *J Physiol* 561, 27-37.

544 Marques, J.M., Rodrigues, R.J., Valbuena, S., Rozas, J.L., Selak, S., Marin, P., Aller, M.I., and Lerma, J. (2013).
545 CRMP2 tethers kainate receptor activity to cytoskeleton dynamics during neuronal maturation. *J Neurosci*
546 33, 18298-310.

547 Mizukawa, K., Tseng, I.M., Otsuka, N. (1998). Quantitative electron microscopic analysis of postnatal
548 development of zinc-positive nerve endings in the rat amygdala using Timm's sulphide silver technique.
549 *Brain Res Dev Brain Res.* 50, 197-203.

550 Morys, J., Berdel, B., Jagalska-Majewska, H., and Luczynska, A. (1999). The basolateral amygdaloid complex-
551 its development, morphology and functions. *Folia Morphol (Warsz).* 58, 29-46.

552 Nair, H.P., and Gonzalez-Lima, F. (1999). Extinction of behavior in infant rats: development of functional
553 coupling between septal, hippocampal, and ventral tegmental regions. *J Neurosci.* 19, 8646-55.

554 Orav, E., Atanasova, T., Shintyapina, A., Kesaf, S., Kokko, M., Partanen, J., Taira, T., and Lauri, S.E. (2017).
555 NETO1 Guides Development of Glutamatergic Connectivity in the Hippocampus by Regulating Axonal
556 Kainate Receptors. *eNeuro* 4(3).

557 Pape, H.C. and Pare, D. (2010). Plastic synaptic networks of the amygdala for the acquisition, expression,
558 and extinction of conditioned fear. *Physiol Rev.* 90, 419-63.

559 Pitkänen, A., Savander, V. and LeDoux, J.E. (1997). Organization of intra-amygdaloid circuitries in the rat: an
560 emerging framework for understanding functions of the amygdala. *Trends Neurosci.* 20, 517–523.

561 Ruiz, A., Sachidhanandam, S., Utvik, J.K., Coussen, F., Mulle, C. (2005). Distinct subunits in heteromeric
562 kainate receptors mediate ionotropic and metabotropic function at hippocampal mossy fiber synapses. *J*
563 *Neurosci.* 25(50), 11710-8.

564 Rutkowska-Wlodarczyk, I., Aller, M.I., Valbuena, S., Bologna, J.C., Prézeau, L., and Lerma, J. (2015). A
565 proteomic analysis reveals the interaction of GluK1 ionotropic kainate receptor subunits with Go proteins. *J*
566 *Neurosci.* 35, 5171-9.

567 Ryan, S.J., Ehrlich, D.E., and Rainnie, D.G. (2016). Morphology and dendritic maturation of developing
568 principal neurons in the rat basolateral amygdala. *Brain Struct Funct.* 221, 839-54.

569 Sah, P., Faber, E.S., Lopez De Armentia, M., and Power, J. (2003). The amygdaloid complex: anatomy and
570 physiology. *Physiol Rev* 83, 803–834.

571 Sallert, M., Malkki, H., Segerstråle, M., Taira, T., and Lauri, S.E. (2007). Effects of the kainate receptor
572 agonist ATPA on glutamatergic synaptic transmission and plasticity during early postnatal development.
573 *Neuropharmacology* 52, 1354-65.

574 Sakha, P., Vesikansa, A., Orav, E., Heikkinen, J., Kukko-Lukjanov, T.K., Shintyapina, A., Franssila, S., Jokinen,
575 V., Huttunen, H.J., and Lauri, S.E. (2016). Axonal Kainate Receptors Modulate the Strength of Efferent
576 Connectivity by Regulating Presynaptic Differentiation. *Front Cell Neurosci.* 10, 3.

577 Segerstråle, M., Juuri, J., Lanore, F., Piepponen, P., Lauri, S.E., Mulle, C., Taira, T. (2010) High firing rate of
578 neonatal hippocampal interneurons is caused by attenuation of afterhyperpolarizing potassium currents by
579 tonically active kainate receptors. *J Neurosci.* 30(19), 6507-14.

580 Shin, R-M., Tully, K., Li, Y., Cho, J.H., Higuchi, M., Suhara, T., and Bolshakov, V.Y. (2010). Hierarchical order
581 of coexisting pre- and postsynaptic forms of long-term potentiation at synapses in amygdala. *PNAS* 107,
582 19073.

583 Tamamaki, N., Yanagawa, Y., Tomioka, R., Miyazaki, J., Obata, K., and Kaneko, T. (2003). Green fluorescent
584 protein expression and colocalization with calretinin, parvalbumin, and somatostatin in the GAD67-GFP
585 knock-in mouse. *J. Comp. Neurol.* 467, 60–79.

586 Tashiro, A., Dunaevsky, A., Blazeski, R., Mason, C.A. and Yuste, R. (2003). Bidirectional regulation of
587 hippocampal mossy fiber filopodial motility by kainate receptors: A two-step model of synaptogenesis.
588 *Neuron* 38, 773.

589 Tottenham, N., and Sheridan, M.A. (2010). A review of adversity, the amygdala and the hippocampus: a
590 consideration of developmental timing. *Front Hum Neurosci.* 3, 68.

591 Tye, K.M., Prakash, R., Kim, S.Y., Fenno, L.E., Grosenick, L., Zarabi, H., Thompson, K.R., Gradinaru, V.,
592 Ramakrishnan, C., Deisseroth, K. (2011). Amygdala circuitry mediating reversible and bidirectional control
593 of anxiety. *Nature* 471, 358.

594 Vesikansa, A., Sakha, P., Kuja-Panula, J., Molchanova, S., Rivera, C., Huttunen, H.J., Rauvala, H., Taira, T., and
 595 Lauri, S.E. (2012). Expression of GluK1c underlies the developmental switch in presynaptic kainate receptor
 596 function. *Sci Rep* 2, 310.

597 Vesikansa, A., Sallert, M., Taira, T., and Lauri, S.E. (2007). Activation of kainate receptors controls the
 598 number of functional glutamatergic synapses in the area CA1 of rat hippocampus. *J Physiol.* 583, 145-57

599 Wilkinson, D.G., and Green, J. (1990). In situ hybridization and the three-dimensional construction of serial
 600 sections. In *Postimplantation Mammalian Embryos*, Copp, A.J., Cockroft, D.L. ed. (IRL Press, Oxford)

601 Wyeth, M.S., Pelkey, K.A., Petralia, R.S., Salter, M.W., McInnes, R.R., McBain, C.J. (2014) Neto auxiliary
 602 protein interactions regulate kainate and NMDA receptor subunit localization at mossy fiber-CA3 pyramidal
 603 cell synapses. *J Neurosci.* 34(2), 622-8.

604 **Figure legends**

605

606 **Figure 1. Kainate receptors are highly expressed in the amygdala during the first postnatal week**

- 607 A. The predominant KAR subunits expressed in the newborn BLA are GluK1, GluK2 and GluK5 and
608 the auxiliary subunit NETO2. RT-aqPCR data on *Grik1-5*, *Neto1* and *Neto2* mRNA expression in
609 the BLA at P4 (n=3-4 rats / group).
- 610 B. RT-qPCR analysis of *Grik1-5*, *Neto1* and *Neto2* mRNA expression in the BLA at different stages
611 of development, expressed as a percentage of the level at P4 (n=3-12 rats / group). *Grik1*
612 expression is strongly downregulated during early postnatal development. *p < 0.05, ** p <
613 0.001 as compared to P4.
- 614 C. Western blot from neonatal (P4 and P14) BLA, using antibodies against GluK2/3 and GluK5.
615 Beta-actin was used as a loading control. GluK2 and GluK5 protein was clearly detected in the
616 BLA both at P4 and P14. Quantification of the signal indicates no significant developmental
617 changes in the expression level. n=3 rats / group.
- 618 D. Cell-type specific expression pattern of KAR subunits in the amygdala during early postnatal
619 development. Example images showing ISH staining (red) with antisense RNA probes against
620 *Grik1*, *Grik2* and *Grik5* mRNA in the P4 mouse amygdala, in GAD67GFP positive (green) and
621 negative (blue DAPI stain) cells. Scale bar, 100 μ m.
- 622 E. Pooled data on the integrated density of the ISH signal, normalized to the number of cell
623 bodies (identified by DAPI staining) within the analyzed region at P4 and P14. *Grik1* mRNA
624 expression is strongly downregulated in all amygdala subnuclei during first weeks of postnatal
625 development. LA, Lateral amygdala; BA Basal Amygdala; CeA Central amygdala (data for each
626 subunit is pooled from n= 3-4 mice and 3 rats). *p < 0.05, ** p < 0.001.
627 See Figure 1 source data for raw values.

628

629 **Figure 2. Development of glutamatergic synaptic connectivity in the amygdala**

- 630 A. Example traces of action-potential independent glutamatergic events (mEPSCs), recorded
631 from LA, BA and CeA neurons at different stages of development.
- 632 B. Pooled data of mEPSC frequency in amygdala subnuclei at different stages of development
633 (n=7-11 from 4-9 rats / group). The mEPSC frequency increases with a different
634 developmental time course in CeA as compared to BA and LA. *p < 0.05, ** p < 0.001.
- 635 C. Confocal images illustrating dendritic spines in biocytin filled neurons from LA, BA and CeA at
636 P5, P10, P15 and P21
- 637 D. Pooled data on spine density in LA, BA and CeA neurons at different stages of development.
638 Data is obtained from 6-10 dendrites from 3 rats/ group. * p < 0.05; ** p < 0.001.
639 See Figure 2 source data for raw values.

640

641

642 **Figure 3. Functional map of ionotropic KAR activity in the amygdala during the first postnatal**
643 **week**

- 644 A. Example traces illustrating inward currents in response to application of 2 μ M kainate (KA) in
645 the presence of blockers for AMPA, NMDA and GABA-A receptors, in LA, BA and CeA neurons
646 at P4-6 and P14-16. 33 mM KCl was applied as a positive control. In the neonatal BLA, no KA
647 induced currents are detected while a clear current is induced under similar conditions at P14-
648 P16.
- 649 B. Pooled data on the effect of 2 μ M kainate on holding current in LA, BA and CeA neurons at
650 two different stages of development (P4-6 and P14-16; LA n= 10 [6] and 13[7]; BA: n=14 [7]
651 and 12 [6], CeA n= 12[10] and 12[8], respectively).
- 652 C. Example traces showing that application of 500 nM of domoate (DA) induced no current in
653 neonate LA neurons, while a small inward current was detected in BA (P4-6). The recordings
654 were made in the presence of blockers for AMPA, NMDA and GABA-A receptors.
- 655 D. Pooled data comparing the effect of or 2 μ M kainate (LA n= 10[4], BA n= 14[4]) and 500 nM
656 domoate (LA: n=10[4]; BA: n=9[4]) on holding current in neonatal LA and BA neurons. The n
657 numbers in this and following figure legends refer to the number of experiments, followed by
658 the number of animals in brackets.
659 See figure 3 source data for raw values.

661 **Figure 4. KARs regulate glutamatergic inputs to BA and CeA during the first postnatal week**

- 663 A. KAR antagonism does not affect action-potential independent glutamatergic events (mEPSCs)
664 to LA during the first postnatal week. Example traces (P5) from the time points indicated (1-3)
665 and time course plot of averaged data (\pm s.e.m.) illustrating little or no effect of ACET (200
666 nM) on mEPSC frequency in LA at P4-7 and at P14-16. The graphs on the right show the
667 mEPSC frequency under control conditions (1), in the presence of ACET (2), and after wash-
668 out of the drug (3), in individual experiments at two different stages of development (P4-7
669 and P14-16; n=7 [4] and 6 [5], respectively).
- 670 B. Similar data for recordings in the BA. In newborn BA, ACET application reversibly increases
671 mEPSC frequency (n= 11[8]). This effect is no longer observed at P14-P16 (n=6[4]). * p < 0.05.
- 672 C. Similar data for recordings in the CeA. In the first week of life (P4-6; n=9[6]) but not at P9-11
673 (n=6[4]), ACET application leads to robust depression of mEPSC frequency. ** p < 0.01.
- 674 D. Scatter plots illustrating the effect of ACET on mEPSC frequency in individual cells in various
675 amygdala subnuclei in the first postnatal week. The P4-7 data from A-C is plotted as a function
676 of the basal mEPSC frequency.
677 Raw data: Figure 4 source data

679 **Figure 5. Transmission at immature BLA-CeA synapses is tonically facilitated by presynaptic G-**
680 **protein coupled KARs.**

681

- 682 A. KAR antagonism leads to reversible depression of glutamatergic transmission from to BLA-CeA
 683 during first postnatal week. Example traces of EPSCs, recorded from CeA neurons at P5 in
 684 response to paired-pulse stimulation of the LA, under control conditions and in the presence
 685 of 200 nM ACET. Pooled data (\pm s.e.m.) showing that ACET application is associated with a
 686 reduction in the EPSC amplitude and an increase in paired pulse ratio. $n = 9$ [5]; $** p < 0.001$.
 687 B. Postsynaptic KARs do not contribute to transmission at immature BLA-CeA synapses. Similar
 688 data as in A, showing that the AMPA receptor antagonist GYKI53655 fully blocks the EPSC. $n =$
 689 8 (4); $p < 0.001$.
 690 C. Example traces from the time points indicated (1-3) and time course plot (average \pm s.e.m.)
 691 depicting a transient increase mEPSC frequency in response to application of KA (500 nM).
 692 The graphs show mEPSC frequency under control conditions (1), in the presence of KA (2), and
 693 after wash-out of the drug (3) in individual cells in CeA (P4-6). $n = 7$ (6); $* p < 0.05$.
 694 D. Application of the GluK1 selective agonist ATPA leads to an increase in mEPSCs frequency,
 695 similar to that observed in response to 500 nM KA. Example traces and pooled data as in C.
 696 $n = 7$ (4); $* p < 0.05$.
 697 E. The tonic KAR activity regulating glutamatergic transmission to CeA acts via a G-protein
 698 dependent mechanism. The effect of ACET on mEPSC frequency is fully blocked in slices that
 699 are pre-incubated in the presence pertussis toxin (PTX; $n = 5$ [3]), but not in SHAM incubated
 700 controls ($n = 5$ [3]). $* p < 0.05$.
 701 See Figure 5 source data for raw values.

702 **Figure 6. Loss of GluK1 in the amygdala in a cKO mouse model impairs glutamatergic innervation**
 703 **and maturation of CeLA neurons**

- 704 A. Image illustrating the GFP fluorescence in the BLA and CeA of *Grik1* cKO mice (P21), after *in*
 705 *vivo* injection of GFP-CRE AAV virus at P2. The viral transduction was mainly targeting LA and
 706 BA (79 ± 5 % and 61 ± 8 % of the DAPI labeled cell bodies (blue), respectively), but also some
 707 cells in the CeA (10 ± 4 % of cells). Scale bar, 100 μ m.
 708 B. Example traces and pooled data showing that loss of GluK1 in the BLA has no effect on the
 709 mEPSCs at LA neurons but results in lower mEPSC frequency and amplitude in the CeLA as
 710 compared to controls. AAV viruses encoding for GFP-CRE or GFP (control) were injected to
 711 the BLA at P2-4, and mEPSCs were recorded from acute slices at P21. LA: GFP $n = 13$ (5), GFP-
 712 CRE $n = 12$ (4); CeLA: GFP $n = 10$ (3), GFP-CRE $n = 11$ (3); $* p < 0.05$.
 713 C. *post hoc* morphological characterization of the biocytin filled CeLA neurons (P21). Density of
 714 dendritic spines was significantly lower in GFP-CRE slices as compared to controls (GFP-CRE,
 715 $n = 11$ (4); GFP $n = 13$ (4)). $** p < 0.01$. Scale bar, 5 μ m
 716 D. Sholl analysis of the same neurons. The number of dendritic intersections and the total
 717 dendritic length is significantly lower in GFP-CRE slices as compared to controls. Pooled data
 718 (GFP-CRE, $n = 11$ (4); GFP $n = 10$ (4)) and confocal images (z-stack) illustrating the morphology
 719 of the dendritic tree. $** p < 0.01$. Scale bar, 50 μ m
 720 E. Local inactivation of *Grik1* at a later developmental stage has no effect on mEPSCs and
 721 dendritic morphology of CeLA neurons. AAV viruses encoding for GFP-CRE or GFP (control)
 722 were injected to the BLA of the *Grik1* cKO mice at P14 and ex vivo analysis was done at P35.

The image panels show mEPSCs (E), dendritic spines (F), intersections and total dendritic length (G) for 7-9(3) neurons from both GFP and GFP-CRE slices.
See Figure 6 source data for raw values.

Figure 6 – figure supplement 1. Validation of the GluK1 cKO mouse model

- A. RT-qPCR results showing loss of *Grik1* mRNA expression in the hippocampus (HC) of *Grik1^{tm1c/tm1c}* mice 23 days after injection of AAV virus encoding for GFP-CRE. Injection was done in 9 week old mice. The data represents the level of *Grik1* mRNA expression in the HC of GFP-CRE group as a percentage of the GFP control (n=3 mice for both groups). * p = 0.01, ANOVA.
- B. Loss of GluK1 function in the LA following injection of AAV virus encoding for GFP-CRE in the *Grik1^{tm1c/tm1c}* mice. Example traces and pooled data illustrating ATPA (1 μ M) induced currents in control (GFP expressing) but not in GFP-CRE expressing LA neurons in acute slices from *Grik1^{tm1c/tm1c}* mice (GFP-CRE: n=4, GFP: n=4; ANOVA; p < 0.05). GFP or GFP-CRE encoding AAV viruses were injected to the BLA of adult *Grik1^{tm1c/tm1c}* mice, acute slices were cut for electrophysiological analysis 21 days after injection. Agonist induced currents were recorded as described in the main article.

Figure 6 – figure supplement 2. Morphological characterization of GFP and GFP-CRE expressing LA neurons in *Grik1* cKO mice

- A. GluK1 deficiency has no significant effect on the density of dendritic spines in LA neurons. AAV viruses encoding for GFP-CRE or GFP (control) were injected to the BLA of GluK1 cKO mice at P2-4 and morphological characterization was performed at P21. Example images and pooled data on the mean density of dendritic spines in GFP-CRE and GFP expressing neurons in the LA (GFP, n= 10(4); GFP-CRE, n= 11(4)). There is no significant difference between the groups (ANOVA, $F_{(1,19)}= 0.697$, p=0.414). Scale bar, 5 μ m.
- B. GluK1 deficiency has no effect on mean dendritic length and branching in LA neurons. Sholl analysis of the biocytin filled LA neurons indicate that number of dendritic intersections and the total dendritic length is not different between GFP and GFP-CRE expressing neurons (GFP, n= 9 (4); GFP-CRE, n=10(4); two-way ANOVA of dendritic intersections $F_{(12,192)}=1.262$, p=0.24; dendritic length ANOVA $F_{(1,17)}=0.874$, p=0.363). Confocal images (z-stack) illustrate the morphology of the dendritic tree. Scale bar, 50 μ m. The n number refers to the number of experiments, followed by the number of animals in brackets.

Figure 6 – figure supplement 3. Development of CeA neuron morphology in control mice and in cKO mice lacking GluK1 in the BLA

- A. Morphological characterization of biocytin filled CeA neurons from WT mice (P6 and P10) and P21 *Grik1* cKO mice, injected with GFP-CRE or GFP (control) encoding AAV viruses to

the BLA at P2-4. Example images and pooled data [P6 n=8(3); P10 n=10(3); P21 GFP n=11(4); P21 GFP-CRE n=13(4)] illustrate developmental increase in spine density from P6 to P10 and from P10 to P21 in control mice (ANOVA $F_{(3,38)}=9.59$, $p<0.001$; Holm-Sidak post-hoc comparison, P6 vs P10 $t=2.567$, $p=0.014$; P10 vs P21 GFP $t=2.803$, $p=0.008$). Following GluK1 inactivation, the spine density at P21 remains similar to P10 WT (Holm-Sidak, P6 vs P21 CRE $t=2.298$, $p=0.027$; P10 vs P21 CRE: $t=0.441$, $p=0.662$). ** $p < 0.01$. Scale bar, 5 μm . The n number refers to the number of experiments, followed by the number of animals in brackets.

B. Sholl analysis of the same neurons. The number of dendritic intersections and the total dendritic length is significantly increased during development from P6 to P21 in control mice (two way ANOVA for dendritic intersections, $F_{(19,418)}=2.89$, $p<0.0001$). Following GluK1 inactivation, the mean dendritic length and branching at P21 remains similar to P6–P10 WT's (dendritic length, ANOVA $F_{(3,35)}=5.724$, $p=0.003$; Holm-Sidak post-hoc comparison P6 vs P10, $t=1.702$, $p=0.098$; P10 vs P21 GFP, $t=1.771$, $p=0.085$; P6 vs P21GFP $t=3.371$, $p=0.002$; P6 vs P21CRE, $t=0.011$, $p=0.991$; P10 vs P21CRE $t=1.835$, $p=0.075$. Dendritic intersections, P10 vs P21CRE, two-way ANOVA $F_{(11,240)}=0.728$, $p=0.71$). Confocal images (z-stack) illustrating the morphology of the dendritic tree. ** $p < 0.01$. Scale bar, 50 μm .

Figure 7. GluK1 deficiency in the amygdala perturbs glutamatergic transmission at LA-CeLA and associates with lower E/I ratio at CeLA late-firing neurons

A. Input – output characteristics of EPSCs, recorded from CeLA neurons in response to LA stimulation. Recordings for all the data presented in panels A-D were made in acute slices from P21 *Grik1* cKO mice, injected with GFP or GFP-CRE encoding AAV viruses in BLA at P2-4. The EPSCs were significantly smaller in slices where GluK1 was locally inactivated as compared to controls. Example traces for responses evoked by 3 different stimulation intensities (0.2, 1 and 2.5 mA) for both groups and pooled data (GFP, n=9[5], GFP-CRE n=8[5], * $p < 0.05$).

B. Example traces and pooled data illustrating the amplitude ratio of AMPAR and NMDAR-mediated EPSCs, evoked by LA stimulation in CeLA neurons. AMPA/NMDA ratio was significantly smaller in GFP-CRE group as compared to GFP controls (GFP n=12[5], GFP-CRE n=13[5], * $p < 0.05$).

C. Paired –pulse ratio of LA-CeLA EPSCs was not different between GFP-CRE and GFP slices. Example traces and averaged data on paired-pulse ratio (PPR) of EPSCs (GFP, n=10[4], GFP-CRE n=10[4]).

D. Example traces of firing pattern of late-firing (LF) and regular-firing (RF) neurons in CeLA (P21) in response to depolarizing current pulses and recordings of spontaneous IPSCs and EPSCs under conditions where the sIPSCs are seen as outward currents and the sEPSCs are directed inwardly. sEPSC frequency was lower in LF neurons in CeLA in animals infected with GFP-CRE encoding AAV viruses at P2-4 as compared to GFP controls. Pooled data on

frequencies of sEPSCs and sIPSCs in RF and LF neurons in CeLA (n=12[4] for both groups, * p < 0.05).

See Figure 7 source data for raw values.

Figure 8. Presynaptic GluK1 KARs guide development of glutamatergic synaptic input to CeA

- A. Image showing GFP expression specifically in the LA at P11, after *in vivo* injection of *Grik1* shRNA/GFP encoding lentivirus at P5. The inset panel shows a magnified image illustrating GFP expression on average of 59 ± 5 % of DAPI labeled (blue) cells in the LA, while practically no expression was detected in the BA (0.7 ± 0.4 %) and CeA (0.1 ± 0.4 %). Scale bar, 100 μ m.
 - B. Example traces and pooled data showing that shRNA mediated GluK1 knockdown in the LA results in lower mEPSC frequency in the CeA as compared to controls. *Grik1* shRNA or mock lentivirus was injected to LA at P5-6 and the recordings were made from CeA neurons at P10-11 (GFP; n=6 (5) ; *Grik1* shRNA/GFP: n=5(3) * p < 0.05).
 - C. Slices with GluK1 overexpression (GluK1 oe) in the LA show a significantly higher mEPSC frequency in the CeA as compared to controls (GFP). *In vivo* transduction was done at P6-9 and recordings were made at P14-15. GluK1 oe, n= 14(5), GFP n= 8(4); * p < 0.05.
 - D. GluK1 oe in the LA recapitulates the developmental phenotype of presynaptic KAR activity. Example traces from the time points indicated (1-3) and time course plots of pooled data illustrate that in GluK1 oe slices, ACET application causes a significant decrease in mEPSC frequency in the CeA neurons (n=5(3), p < 0.05). At this developmental stage (P14-15), ACET has no effect on mEPSCs in control (GFP infected) slices (n=5(3)). Graphs on the right show mEPSC frequency under control conditions (1), in the presence of KA (2), and after wash-out of the drug (3) in individual cells. * p < 0.05, paired t-test.
 - E. GluK1 oe results in an increase in dendritic length and branching. Sholl analysis of the biocytin filled CeA neurons indicate that number of dendritic intersections and the total dendritic length is significantly increased in slices with GluK1 oe in the LA. Pooled data (GluK1 oe, n= 6 (3); GFP n=7(3)) and confocal images (z-stack) illustrating the morphology of the dendritic tree. ** p < 0.01. Scale bar, 50 μ m.
 - F. GluK1 oe does not influence the density of dendritic spines in CeA neurons. Pooled data of the mean density of dendritic spines (GluK1 oe n=7(4); GFP, n= 9(4)). Example images shown on the right. Scale bar, 5 μ m.
- See Figure 8 source data for raw values.

Figure 8 – figure supplement 1. Validation of the *Grik1* shRNA

- A. A western blot illustrating that the *Grik1* shRNA strongly inhibits expression of GluK1-myc but not GluK2-myc or GluK3-myc in HEK293T cells.
- B. RT-qPCR results showing that the lentiviral *Grik1* shRNA construct blocks expression of endogenous GluK1 in dorsal root ganglion (DRG) neurons within 48 h from infection.

Materials and Methods

Animals

Male and female Wistar rats (P4-P21) were used in most experiments. Heterozygous *Grik1tm1a*(KOMP)Mbp mice in C57BL/6N background were obtained from KOMP repository (UC Davis) and intercrossed to generate *Grik1^{tm1a/tm1a}*. *Grik1^{tm1a/tm1a}* mice were crossed with CAG-Flp transgenic line to produce a floxed conditional allele (tm1c). Progeny homozygous for the tm1c allele (*Grik1^{tm1c/tm1c}*) was used for further breedings and experiments. Loss of *Grik1* mRNA expression after injection of GFP-CRE encoding AAV virus was validated using qPCR and loss of function was confirmed with electrophysiological analysis (Figure 6-Supplement 1). All experiments were done in accordance with the guidelines given by the ethics committee for animal research at the University of Helsinki.

RNA extraction, cDNA synthesis and real-time PCR. The BLA was dissected from 500 µm thick sections cut from the brain of Wistar rats as described (Lauri et al., 2006). Purification of total RNA, cDNA synthesis and the real-time quantitative PCR was carried out essentially as described (Orav et al., 2017) and using the primers listed in Table 1. All samples were analysed in triplicate. The initial mRNA copy numbers of a sample was obtained by relating the Ct of the sample to a standard curve plot. Relative quantification of gene expression at different developmental stages was analysed using standard 2^{-ddCt} method.

Table 1. Real-time PCR primers

Target	Forward	Reverse	size bp
<i>Grik1</i>	ATGTGACGCAGAGGAACTGC	GCAGTTGAAGAATGGCAATCG	126
<i>Grik2</i>	GTTTGTACACAGCGGAACTG	CAGCTGAAGAATTGCTATGGTG	127
<i>Grik3</i>	CATCGATTCCAAGGGCTACG	CGCCACCACTTCTCCTTCAT	126
<i>Grik4</i>	GACACCAAGGGCTATGGGAT	ACCACTTCCGCTTCAGAATC	118
<i>Grik5</i>	AGTACGGCACTATCCACGCT	CTCCTCTGTGCTCTTGACGA	128
<i>Neto1</i>	TCATAGAAGCTGCCCCAAGG	AAGCCAAAGGGTCCATCTCG	118
<i>Neto2</i>	TTTGAAGCTGCTCCTCGTC	TCCAAGTGATCAAACCGGCA	93
<i>Gadph</i>	CAGTGCCAGCCTCGTCTCATA	TGGTAACCAGGCGTCCGATA	79

Western blotting. Eight P4 rats and six P14 rats were used for measuring the protein levels of the GluK2/3, and GluK5 subunits in the BLA. BLA was dissected from 500 µm thick brain sections and the tissue was sonicated in lysis buffer (1% NP-40, 20 mM Tris, pH 8.0, 137 mM NaCl, 10% glycerol, Phosphatase Inhibitor Cocktails; Upstate, Temecula, CA, USA). Cellular debris was removed by centrifugation. Protein concentrations were measured by a colorimetric DC Protein Assay (Bio-Rad, USA). 60 µg of each sample from each brain region were used in the analysis in triplicate. Proteins were separated on 4-15% Mini-Protean TGX Gel (Bio-Rad, USA) and transferred to PVDF membranes (Millipore). After blocking with 4% non-fat dry milk in PBS for 1 h, the membranes were incubated overnight at 4°C with specific primary antibodies, diluted in 2% non-fat dry milk in

875 PBS as follows: anti-GluR6/7 (GluK2/3), (1:2000; Millipore), KA2 (GluK5) (1:2000; Millipore), and
876 anti-beta-actin (1:10000; Sigma-Aldrich), which was used as a loading control in all experiments.
877 After washing in PBS-T, membranes were incubated with peroxidase-conjugated goat anti-rabbit
878 (1:5000; Bio-Rad, USA) or goat anti-mouse (1:5000; Bio-Rad, USA) secondary antibodies (2% non-
879 fat dry milk in PBS; 1h at RT). After washing in PBS-T, blots were developed using enhanced
880 chemiluminescence with Pierce ECL Western Blotting Substrate (Thermo Scientific). Intensity of
881 the bands was analysed using ImageJ software and normalized relative to the beta-actin.

882 **In situ hybridization (ISH).** ISH was carried out on 5 µm thick paraffin sections from rat and mouse
883 (GAD67-GFP knock-in; Tamamaki et al., 2003) brain as described (Wilkinson and Green, 1990). The
884 digoxigenin (DIG)-labeled antisense and sense RNA probes against *Grik1*, *Grik4*, *Grik5*, *Neto1* and
885 *Neto2* mRNAs, encoding for KAR GluK1, GluK4, GluK5, NETO1 and NETO2, were as previously
886 described (Vesikansa et al., 2012; Orav et al., 2017). *Grik2* cDNA was amplified by PCR using the
887 following primers: Forward GGATGTGATCAGTCTCAAGG, Reverse AGCCAGCAGAACATACATCC. The
888 fragment (532 bp) was subcloned into pGEM-T vector (Promega). The plasmid was linearized by
889 restriction digest and used as a template for *in vitro* transcription with DIG RNA Labeling kit (Roche
890 Diagnostics).

891 TSA-Plus Cyanine3 /Fluorescein System (Perkin Elmer) was used to visualize ISH signal, followed
892 with a standard DAPI staining. In GAD67-GFP knock-in mouse sections, the primary antibody
893 against GFP (rabbit anti-GFP ab290, Abcam) was added after the ISH signal detection to amplify
894 the GFP signal. Stained sections were imaged using Zeiss Axioimager M2 microscope with AxioCam
895 HRc camera.

896 The specificity of reaction conditions was first tested in P14 rat hippocampal sections, to ensure
897 specific staining with anti-sense probe and to control that there was no unspecific signal with the
898 corresponding sense RNA probes (Vesikansa et al., 2012). The level of mRNA expression in the
899 amygdala nuclei was quantified based on the optical density of the ISH signal within anatomically
900 defined area, which was normalized against the quantity of cells (DAPI staining) using ImageJ
901 software. mRNA expression level in hippocampal CA3 region was examined as a reference. For the
902 histograms, data from rat and mouse sections have been pooled as no major differences in the
903 expression pattern between the species were detected. At least 3 sections were analysed for each
904 animal, and at least 3 animals were included in each group.

905 **Electrophysiology.** Acute coronal sections (300-400 µm) were prepared from brains of neonatal
906 (P4-P6) or juvenile (P14-P21) rats or GriK1^{tm1c/tm1c} mice (P21) using standard methods (Lauri et al.,
907 2006). After recovery, the slices were transferred to a submerged recording chamber and
908 superfused with extracellular solution (ACSF) containing (mM): 124 NaCl, 3 KCl, 1.25 NaH₂PO₄, 1
909 MgSO₄, 26 NaHCO₃, 15 D-glucose, 2 CaCl₂; 5 % CO₂ / 95% O₂, at 30°C. Whole-cell patch clamp
910 recordings were performed from BLA and CeA neurons under visual guidance using patch
911 electrodes with resistance of 3–5 MΩ. Uncompensated series resistance (Rs) was monitored by
912 measuring the peak amplitude of the fast whole-cell capacitance current in response to a 5 mV
913 step. Only experiments where Rs < 30 MΩ, and with < 20 % change in Rs during the experiment,
914 were included in analysis.

915 Kainate and domoate induced currents were recorded in the presence of antagonists for AMPA,
916 NMDA and GABA-A receptors (2 μ M NBQX, 50 μ M D(-)-2-amino-5-phosphonopentanoic acid (D-
917 AP5) and 100 μ M picrotoxin (PiTX), respectively) using intracellular solution containing (in mM):
918 135 K-gluconate, 10 HEPES, 5 EGTA, 4 Mg-ATP, 0.5 Na-GTP, 2 KCl, and 2 Ca(OH)₂ (285 mOsm), pH
919 7.2. The agonists were applied using fast local application to the slice and washed out by fast local
920 application of ACSF; following application of ACSF with 33 mM KCl was used as a positive control.

921 Glutamatergic synaptic currents were recorded using Cs-based intracellular solution containing (in
922 mM): 130 CsMeSO₄, 10 HEPES, 0.5 EGTA, 4 Mg-ATP, 0.3 Na-GTP, 5 QX-314, 8 NaCl; 280 \pm 5 mOsm
923 (pH 7.2). For post-hoc morphological analysis, biocytin (0.4 %) was included in the intracellular
924 solution in some of the recordings. Spontaneous miniature EPSCs (mEPSCs) were recorded in the
925 presence of TTX (1 μ M), and PiTX (100 μ M) at a holding membrane potential of -70 mV. mEPSCs
926 were analyzed with MiniAnalysis 6.0.3 program (Synaptosoft Inc.). Events were verified visually,
927 and events with amplitude less than three times the baseline rms noise level were rejected. For
928 time-course plots, detected events were calculated in 120-s bins. Pertussis toxin (PTX) treatment
929 was performed with acute slices at 37° C for 3-5 hours. In these experiments, slices were washed
930 with 1 mL incubation solution containing (in mM): 105 NaCl, 3 KCl, 1 MgSO₄, 3.75 NaH₂PO₄, 26
931 NaHCO₃, 2 CaCl₂, 15 D-glucose, and 25 HEPES (pH = 7.2) with or without 5 μ M PTX, and placed into
932 Millicell CM 0.4- μ m membrane inserts (Millipore) with 1 mL of the above solution.

933 Evoked EPSCs were recorded at a holding membrane potential of -70 mV in response to
934 stimulation of LA by a bipolar metal electrode in the presence of PiTX (100 μ M) D-AP5 (50 μ M).
935 Stimulus-response curves were obtained by applying stimuli with fixed intensities, between 0.2-2.5
936 mA. Paired pulse responses were evoked with 50 ms inter-pulse interval. For AMPA-NMDA ratio,
937 evoked EPSCs were recorded in the presence of PiTX at -70 and +40 mV. The AMPAR-related
938 component was calculated as the peak of the response at -70 mV, and NMDAR-mediated current
939 was isolated by calculating the average amplitude of the response recorded at +40 mV 50–60 ms
940 after stimulation. Data were collected and analyzed online using LTP software (Anderson and
941 Collingridge, 2007; www.winltp.com).

942 Spontaneous glutamatergic and GABAergic synaptic events (sEPSCs and sIPSCs) were recorded
943 using intracellular solution containing (in mM): 135 K-gluconate, 10 HEPES, 2 KCl, 2 Ca(OH)₂, 5
944 EGTA, 4 Mg-ATP, and 0.5 Na-GTP. After obtaining whole cell access, the firing properties of the cell
945 were identified by applying a current injections (600 ms, increments of 20 pA from -100 to 300
946 pA) in current clamp mode. Then the cell was voltage clamped to -50 mV for recording of
947 spontaneous synaptic activity. AP threshold and delay were analyzed off-line.

948 For all the electrophysiological data, n number refers to the number of recorded neurons, which in
949 all datasets were collected from at least 3 (in most cases from at least 6) different animals. The
950 number of animals used in each dataset is indicated in brackets after the n value. Data obtained
951 from the genetically manipulated mice were analyzed by researcher blind to the type of virus
952 infection.

953 **Morphological analysis.** For *post hoc* morphological characterization of biocytin filled neurons,
954 slices were fixed overnight in a 4% paraformaldehyde (4°C), after which they were washed with

955 0.01 M phosphate-buffered saline (PBS) and permeabilized with 0.01 M PBS 0.3% Triton-X 100
956 (Sigma-Aldrich) for 1.5 h at room temperature. Streptavidin Conjugate (1:500; A488; Life
957 Technologies) was added to the permeabilization solution and incubated for 4 h. PBS-washed
958 slices were mounted onto slides and blind-coded for morphological analysis. Dendritic trees and
959 dendritic spines were imaged using a LSM Zeiss 710 confocal microscope (Zeiss Plan Neofluar
960 20x/0.50 and alpha Plan146 Apochromat 63x/1.46 OilKorr M27 objectives). Dendritic trees
961 were imaged with resolution of 2.3 pixels/ μ m and Z-stack interval of 1 μ m. Spines were imaged
962 with resolution of 15.17 pixels/ μ m and Z-stack interval of 0.5 μ m. Spine density was evaluated
963 on the primary dendrites for P7-11 and on the secondary for P14-21. Actual spine detection
964 was done using the NeuronStudio software to quantify spines in a Z-stack image. Verification of
965 the spine detection was done manually. Values of spine density per cell were used for statistical
966 analysis. Sholl analysis was performed on 2D maximal intensity images acquired from Z-stacks,
967 using the Fiji ImageJ plugin. The number of intersections was estimated with 10 μ m bins, and
968 values per cell were used for statistical analysis. Total dendritic length were measured from
969 traced dendrites of each cell.

970 **Viral transduction *in vivo*.** Lentiviral vectors encoding epitope-tagged GluK1 were as described
971 previously (Vesikansa et al., 2012). The shRNA against GluK1 (target sequence:
972 CCTGGACATTATCAGTCTCAA) was subcloned to modified pLKO.1 vector where the puromycin
973 resistance cassette was replaced with GFP under the synapsin-1 promoter (pLKO.1- syn1-EGFP).
974 The lentiviral particles were produced in HEK293T cells and purified as described (Vesikansa et al.,
975 2012). The efficacy of the lentiviral shRNA to suppress expression of GluK1 was validated in
976 cultured DRG cells, where GluK1 is endogenously strongly expressed (Figure 8 – figure supplement
977 1). Lentiviral particles were injected to the LA area of 4–5 day old rat pups (for shRNA) and 6-9 day
978 old pups (for overexpression) under isoflurane anesthesia. The animals were placed onto
979 stereotaxic frame, the skull was exposed and 2 or 3 small holes at each side were done using
980 dental drill. 0.3-0.6 ml of lentiviral suspension was injected into LA region of amygdala. The
981 stereotaxic coordinates for LA were recalculated in the respect to bregma – lambda distance and
982 varied in the following range for P5-6: AP 1.2, 2.0, 2.8 (from bregma), ML 3.8–3.9, DV 3.6–3.8; and
983 for P6-9: AP 2.0, 2.8 (from bregma), ML 4.5–4.6, DV 6–6.2. The wound was stitched and treated
984 with bacibact (Orion Pharma, Finland), sutured and the pup was left to recover with the dam.

985 AAV serotype 8 vectors encoding for GFP (pAAV.CMV.PI.EGFP.WPRE.bGH) and GFP-CRE
986 (pAAV.CMV.HI.eGFP-Cre.WPRE.SV40) were purchased from Addgene (catalog #105530-AAV8 and
987 105545-AAV8, respectively). The AAV particles were injected to the BLA of neonatal (P1-4)
988 *Grik1^{tm1c/tm1c}* mice under anaesthesia in a stereotaxic frame as described above, except that the
989 injection was done through the skin and skull using the following coordinates: AP 3.8 (from the
990 most rostral point) ML 2.2, DV 2.2.

991 The specificity of the injection site was visually monitored after preparation of the acute slices for
992 electrophysiological recordings. Only slices with 1) strong GFP signal in the LA and 2) no visible GFP
993 signal in the CeA (lentiviral injections) or estimated CeA GFP intensity < 20 % of the level in LA
994 (AAV injections) were included in further analysis. The exact infection rate in different amygdala

995 nuclei was quantified using slices from 3 animals that had passed the visual inspection criteria. The
996 percentage of GFP positive neurons from all DAPI positive cells in LA, BA and CeA was calculated
997 from Z-stack confocal images (8-12 images with interval of 10 μ m).

998 **Statistical analysis.** All statistical analysis was done on raw (not normalized) data using Sigma Plot
999 11.0 or Graph Pad Prism 8.0.2 software. To analyse differences between groups, Shapiro-Wilk test
1000 was used to test for normal distribution and one-way ANOVA with Holm-Sidak post hoc
1001 comparison or one-way ANOVA on ranks (Kruskal-Wallis with Dunn's method for pairwise
1002 comparison) was then used accordingly. For pharmacological effects, Student's paired two-tailed
1003 t-test or Wilcoxon rank sum test was used. The test as well as the corresponding F, H, t and Z
1004 values are indicated in the text, with the degree of freedom as subscript. The results were
1005 considered significant when $p < 0.05$. All the pooled data are given as mean \pm S.E.M.

1006

1007

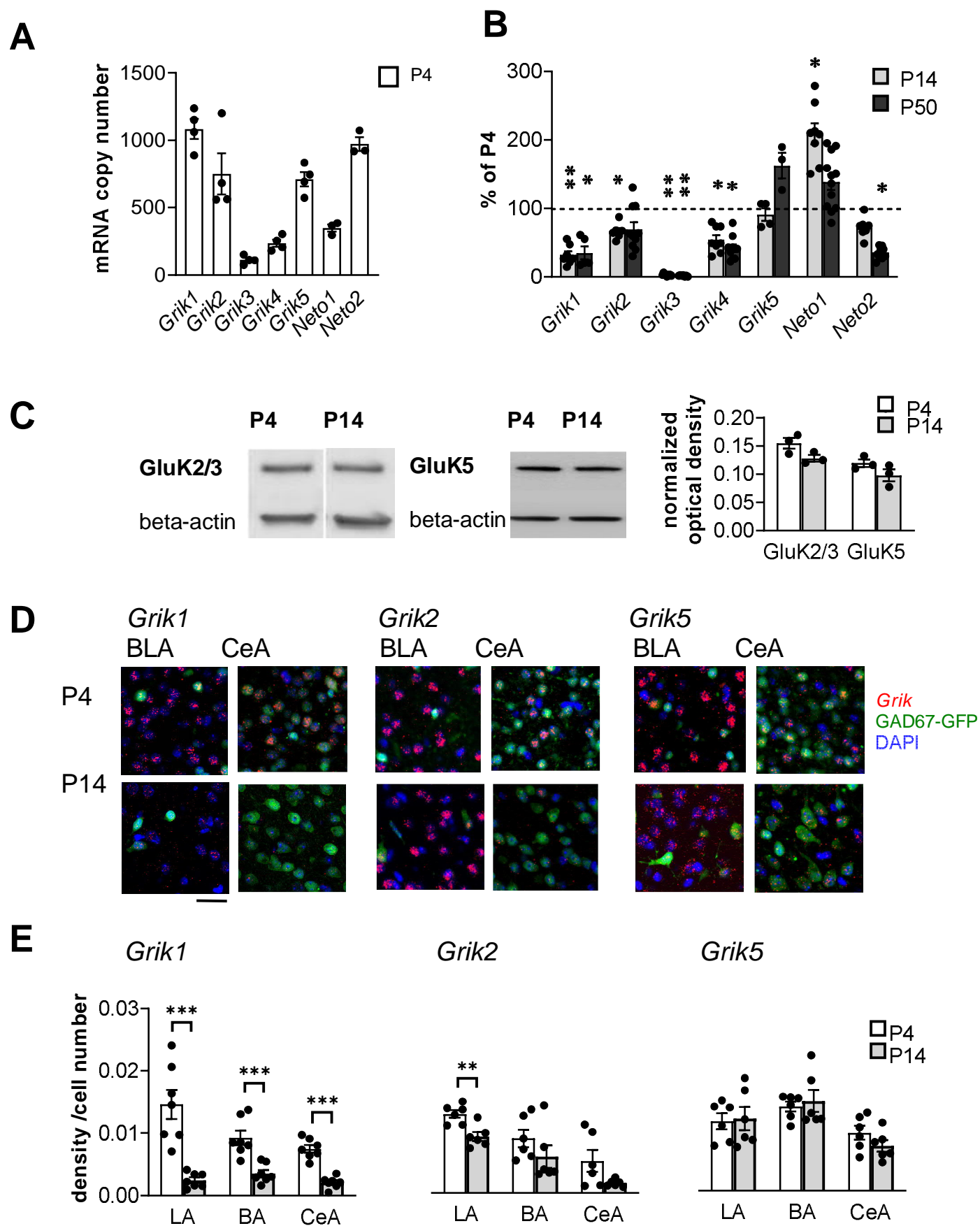
Figure 1

Figure 2

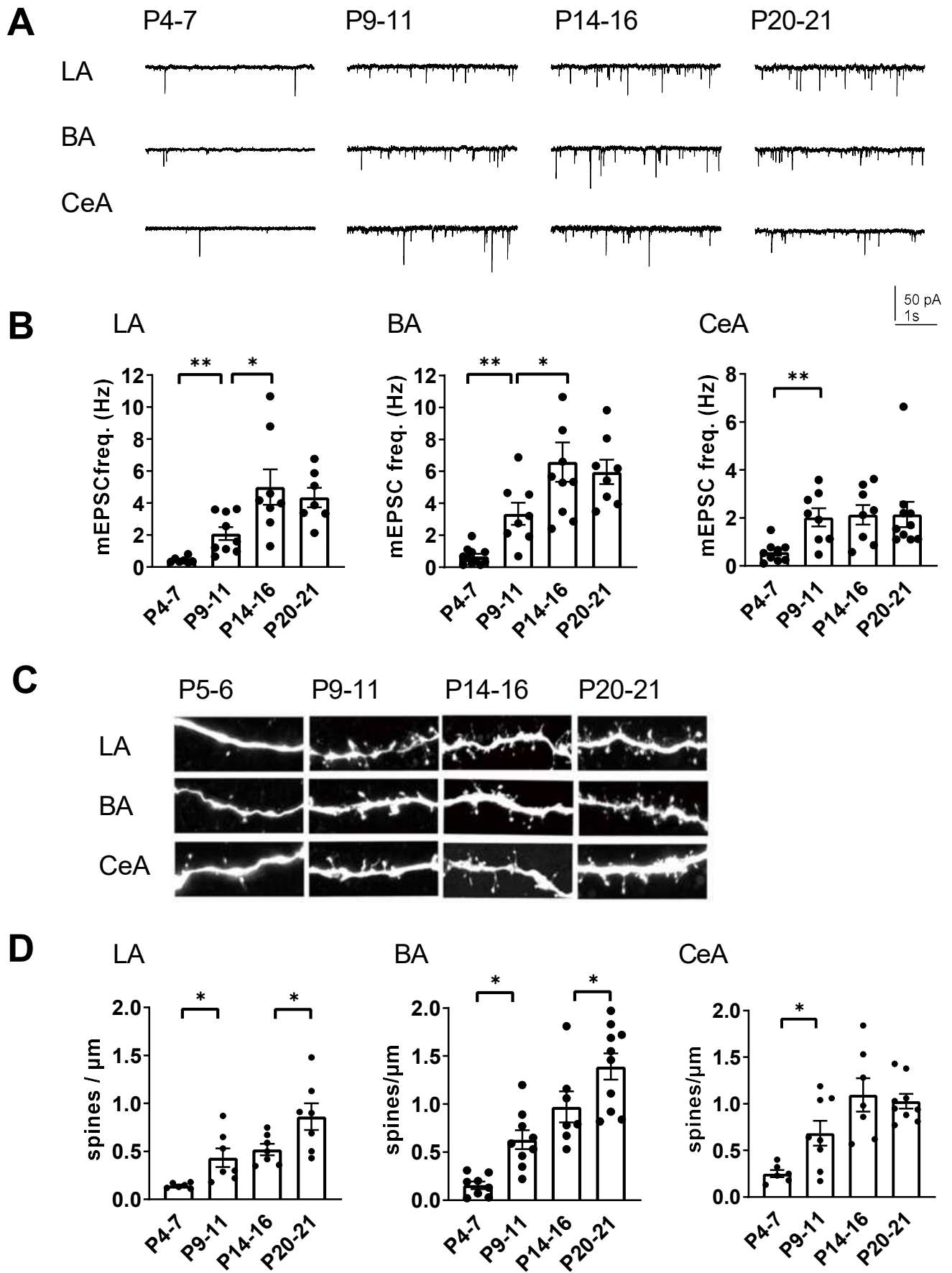


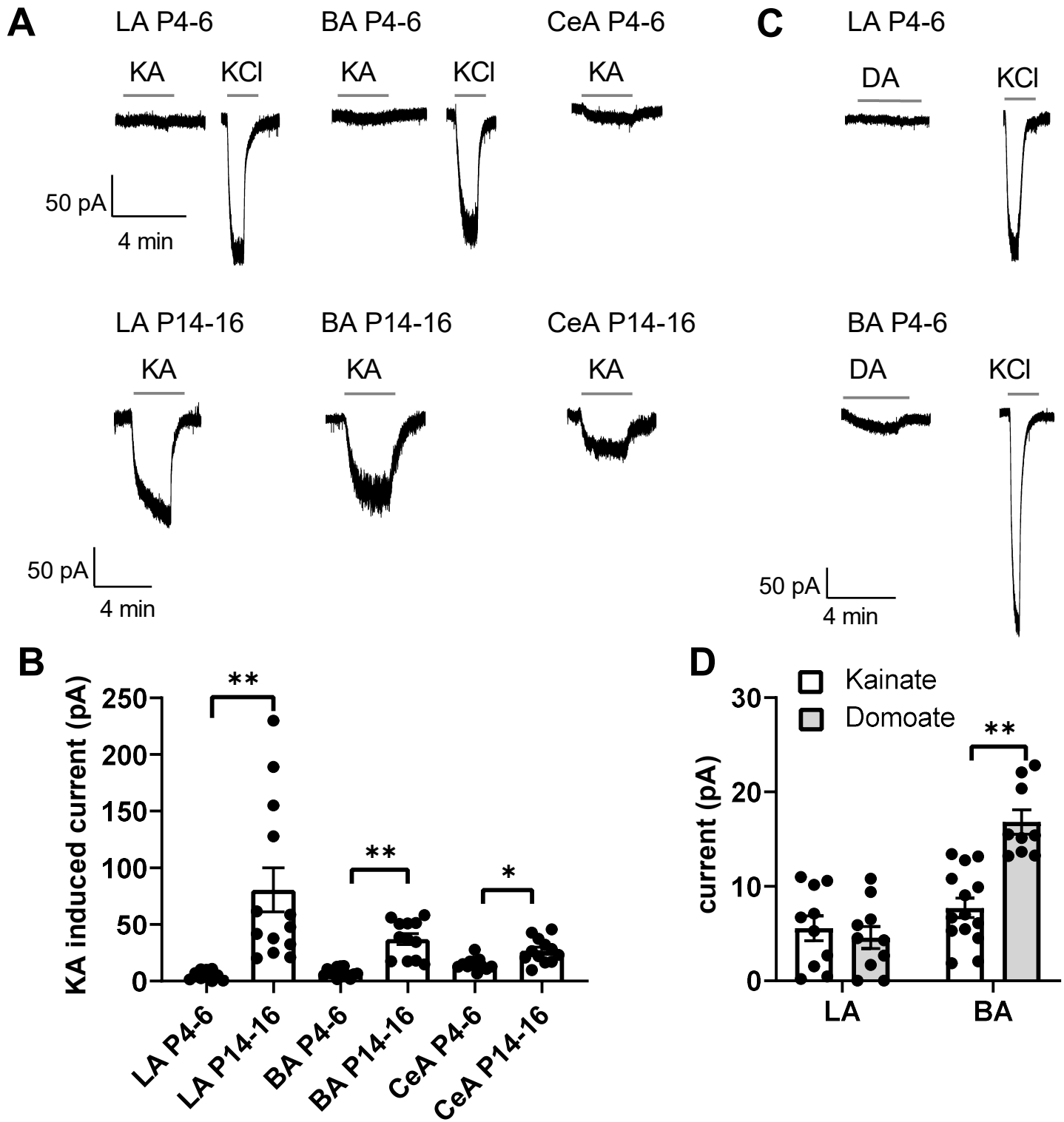
Figure 3

Figure 4

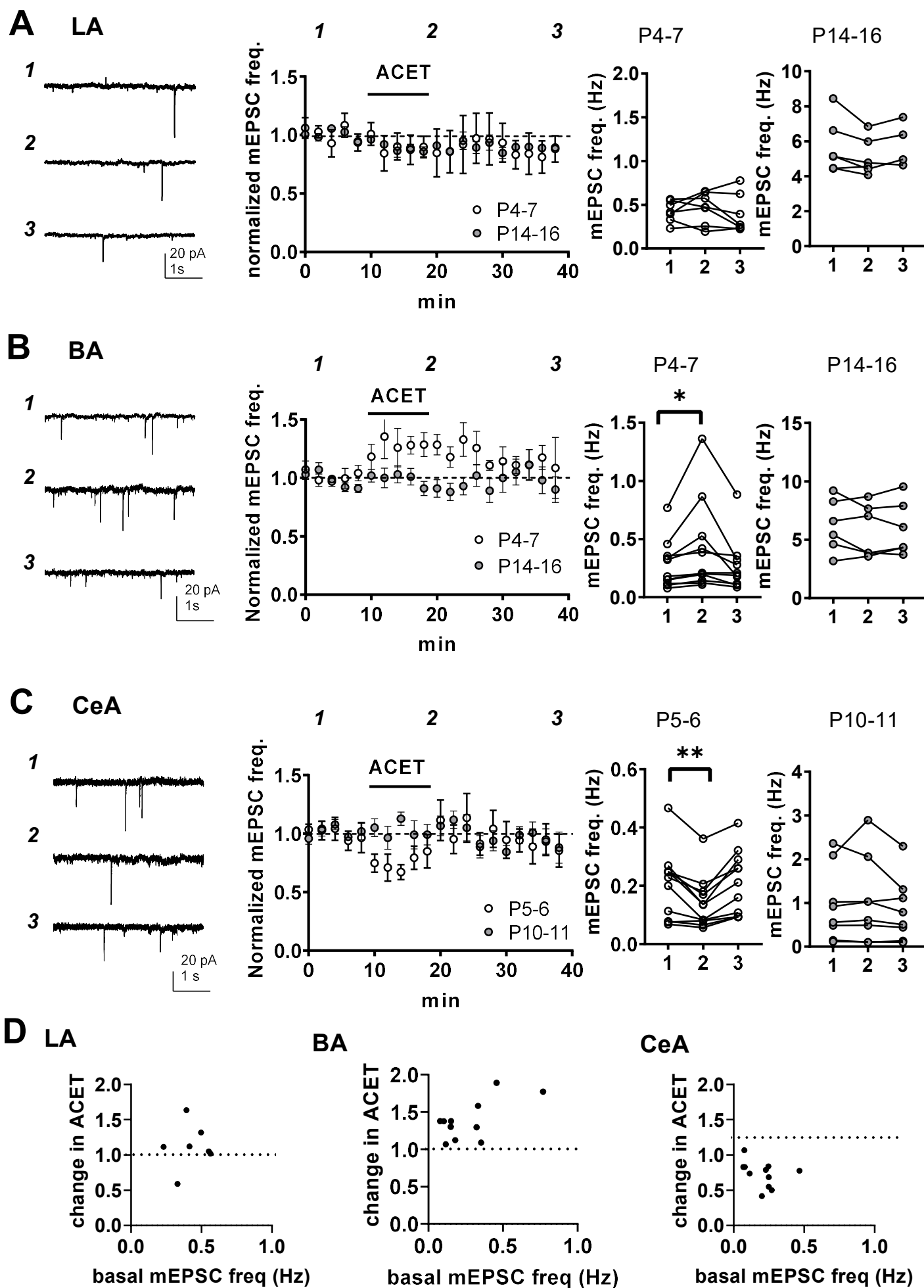


Figure 5

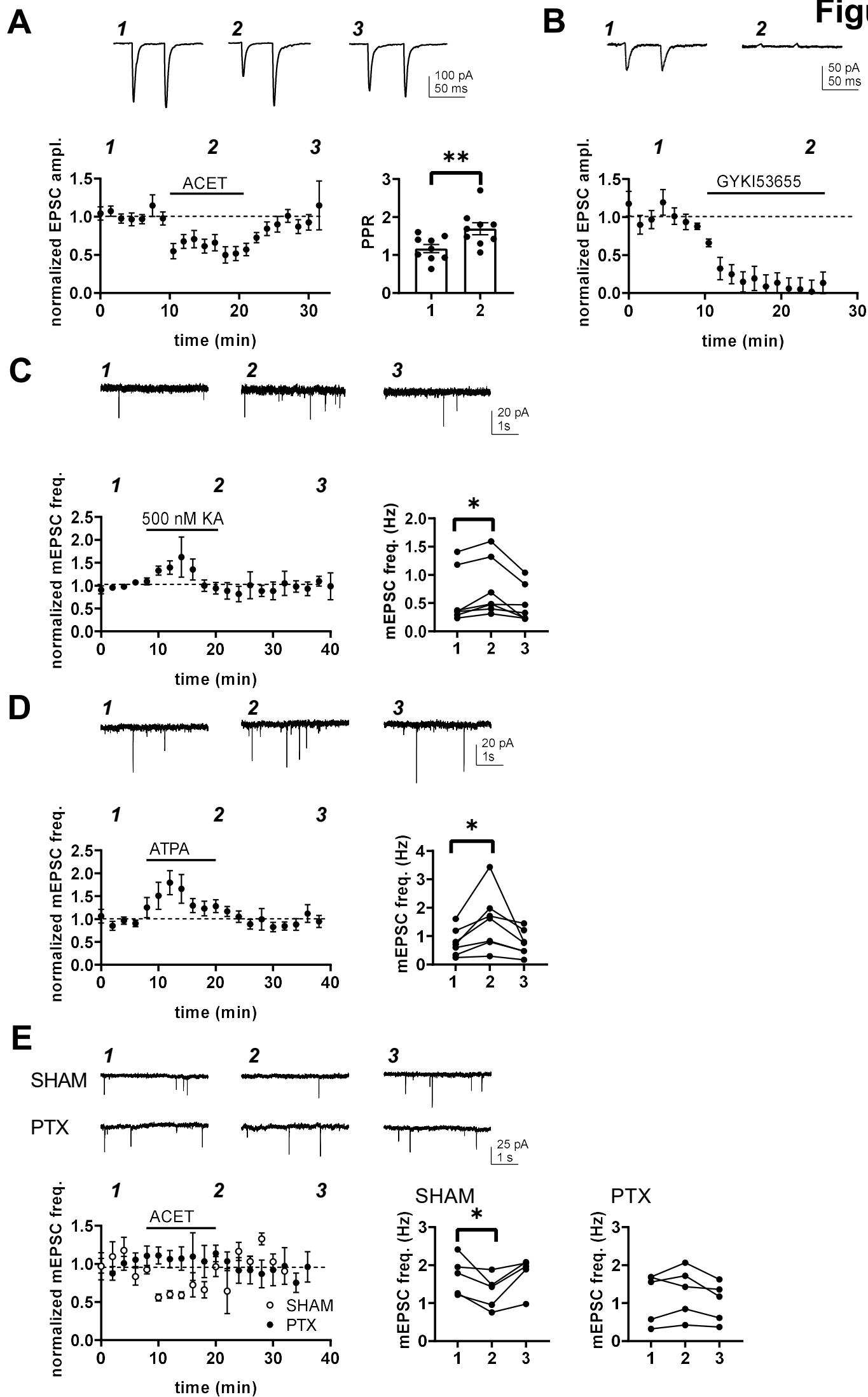


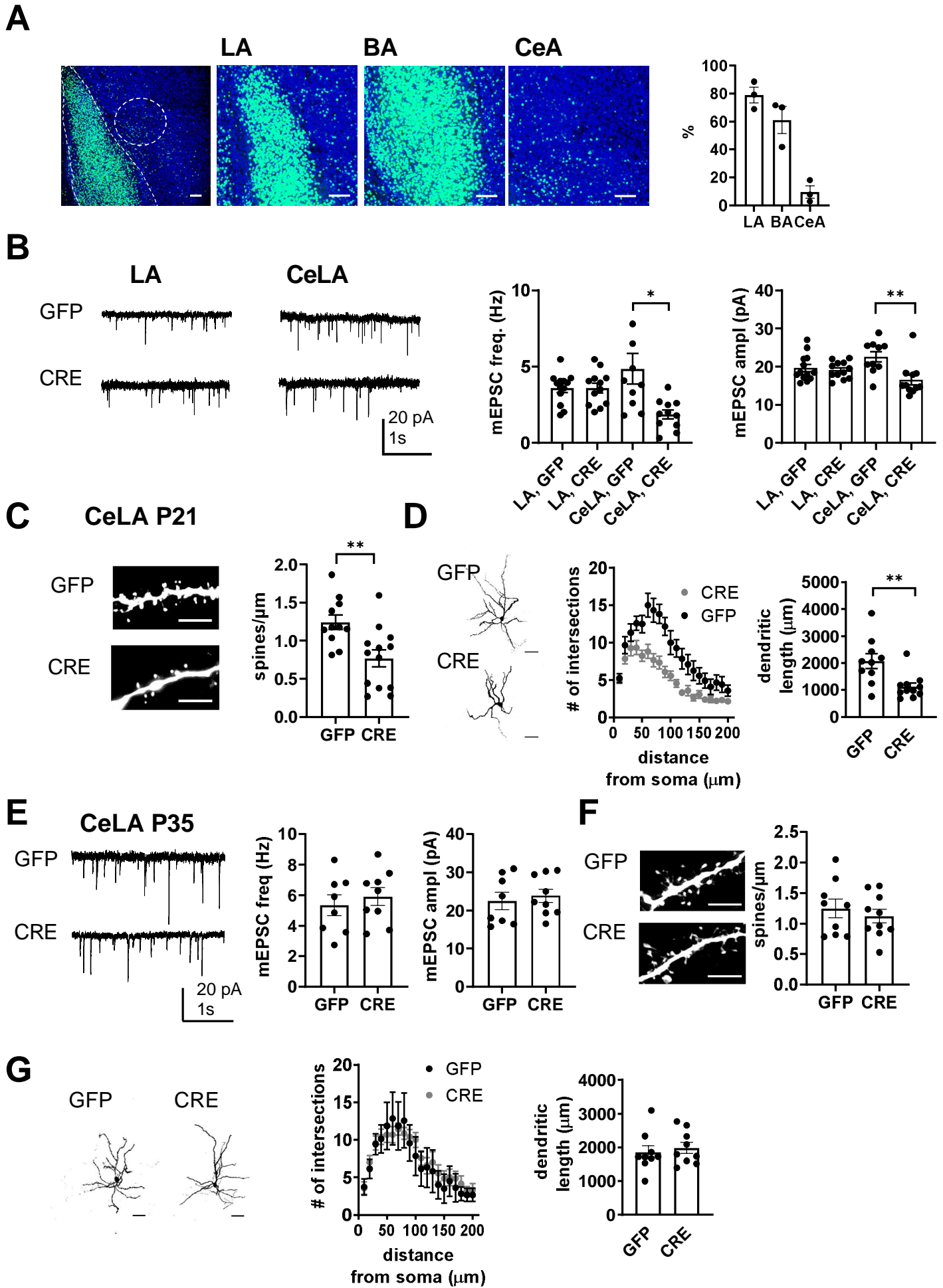
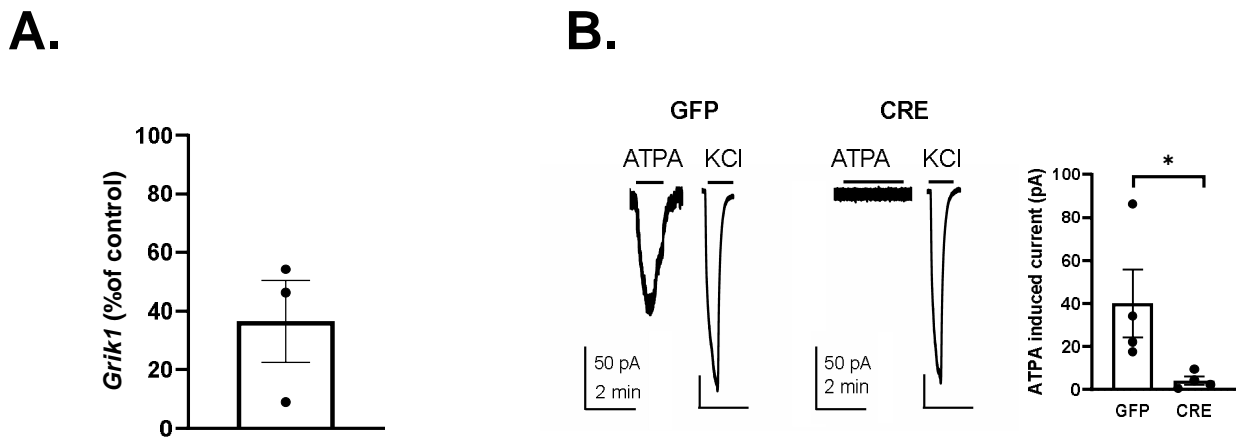
Figure 6

Figure 6 – figure supplement 1



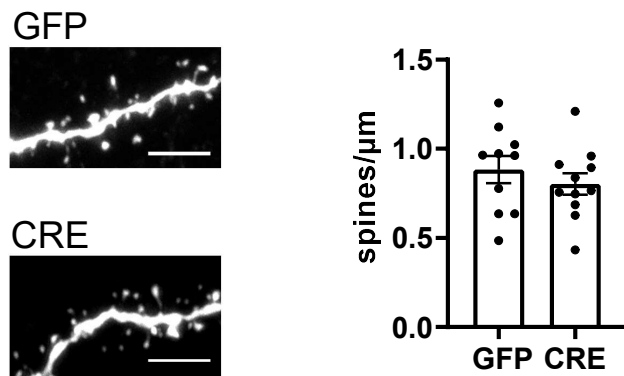
Validation of the GluK1 cKO mouse model

- A. RT-qPCR results showing loss of Grik1 mRNA expression in the hippocampus (HC) of Grik1^{tm1c/tm1c} mice 23 days after injection of AAV virus encoding for eGFP-Cre. Injection was done in 9 week old mice. The data represents the level of Grik1 mRNA expression in eGFP-Cre – injected HC as a percentage of the control (eGFP injected HC, n=3 for both groups) . * p < 0.05, unpaired t-test.
- B. Loss of GluK1 function in the LA neurons following eGFP-Cre injection in the Grik1^{tm1c/tm1c} mice. Example traces and pooled data illustrating ATPA (1 μM) induced currents in LA neurons in slices obtained from control (eGFP injected) but not in eGFP-Cre injected Grik1^{tm1c/tm1c} mice (eGFP-Cre: n=4, eGFP: n=4; ANOVA; p < 0.05). eGFP or eGFP-Cre encoding AAV viruses were injected to the BLA of adult Grik1^{tm1c/tm1c} mice, acute slices were cut for electrophysiological analysis 21 days after injection. Agonist induced currents were recorded as described in the main article.

Methods for the RTqPCR. The whole hippocampi were dissected from the Grik1^{tm1c} mice, and stored in RNALater stabilization solution. RNA extraction and purification was done using the RNeasy Mini Kit (Qiagen), any remaining DNA was removed using DNA-free DNA Removal Kit (Thermo Fisher Scientific), and cDNA synthesis was carried out using RevertAid First Strand cDNA Synthesis Kit (Thermo Fisher Scientific) with oligo(dT)18 primers. Real-time quantitative PCR was done using forward primer AAAGTGGTTCCTGACGGCAA and reverse primer CTGCTAGGTCAGCTCTGTGG. All samples were analysed in triplicate, and relative quantification of gene expression was analysed using the 2- $\Delta\Delta C_t$ method.

Figure 6 - figure supplement 2

A



B

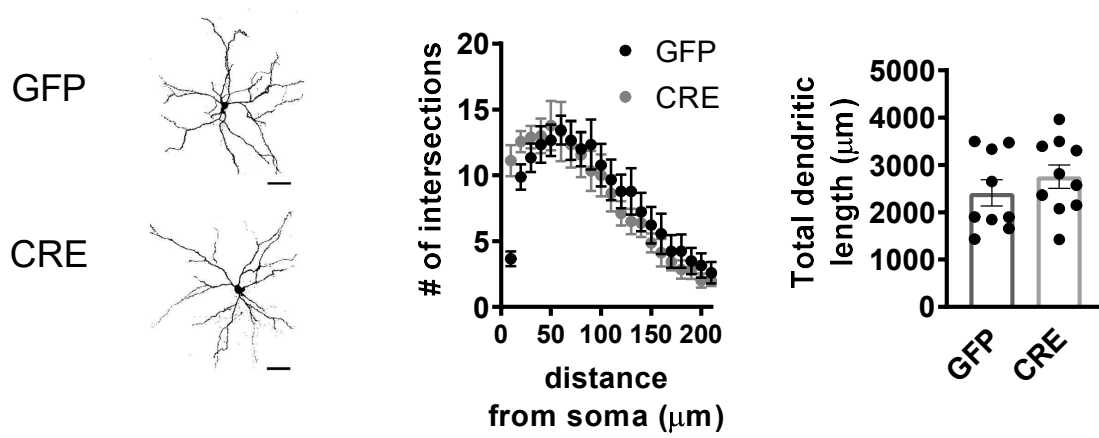
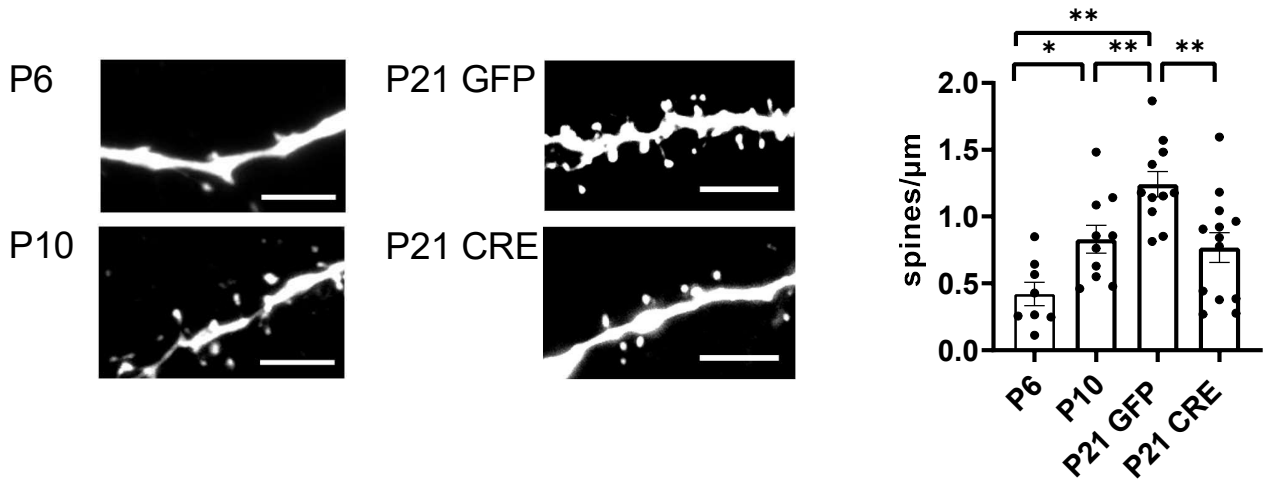


Figure 6 - figure supplement 3

A



B

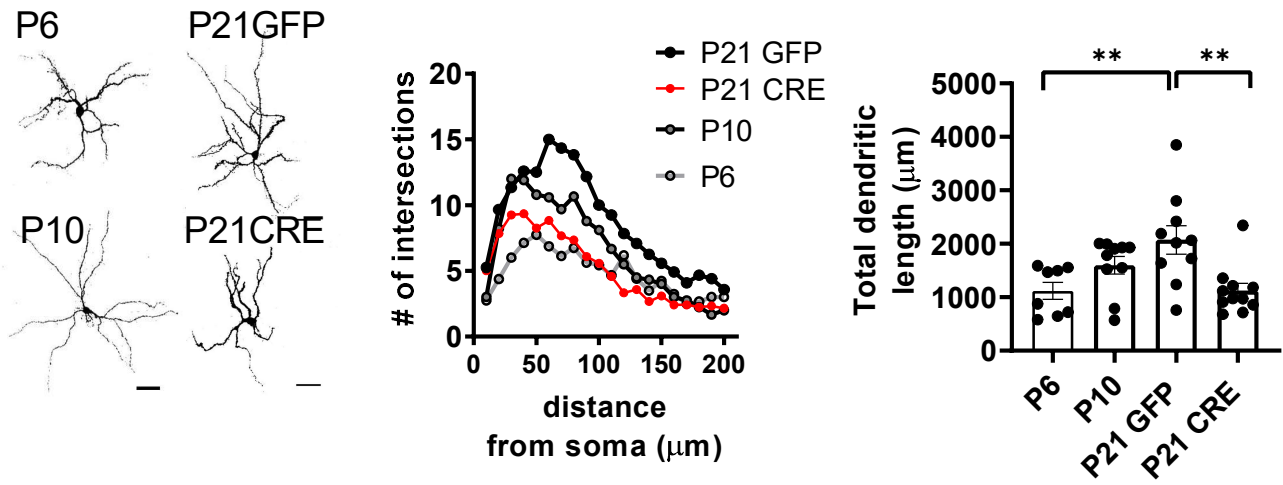


Figure 7

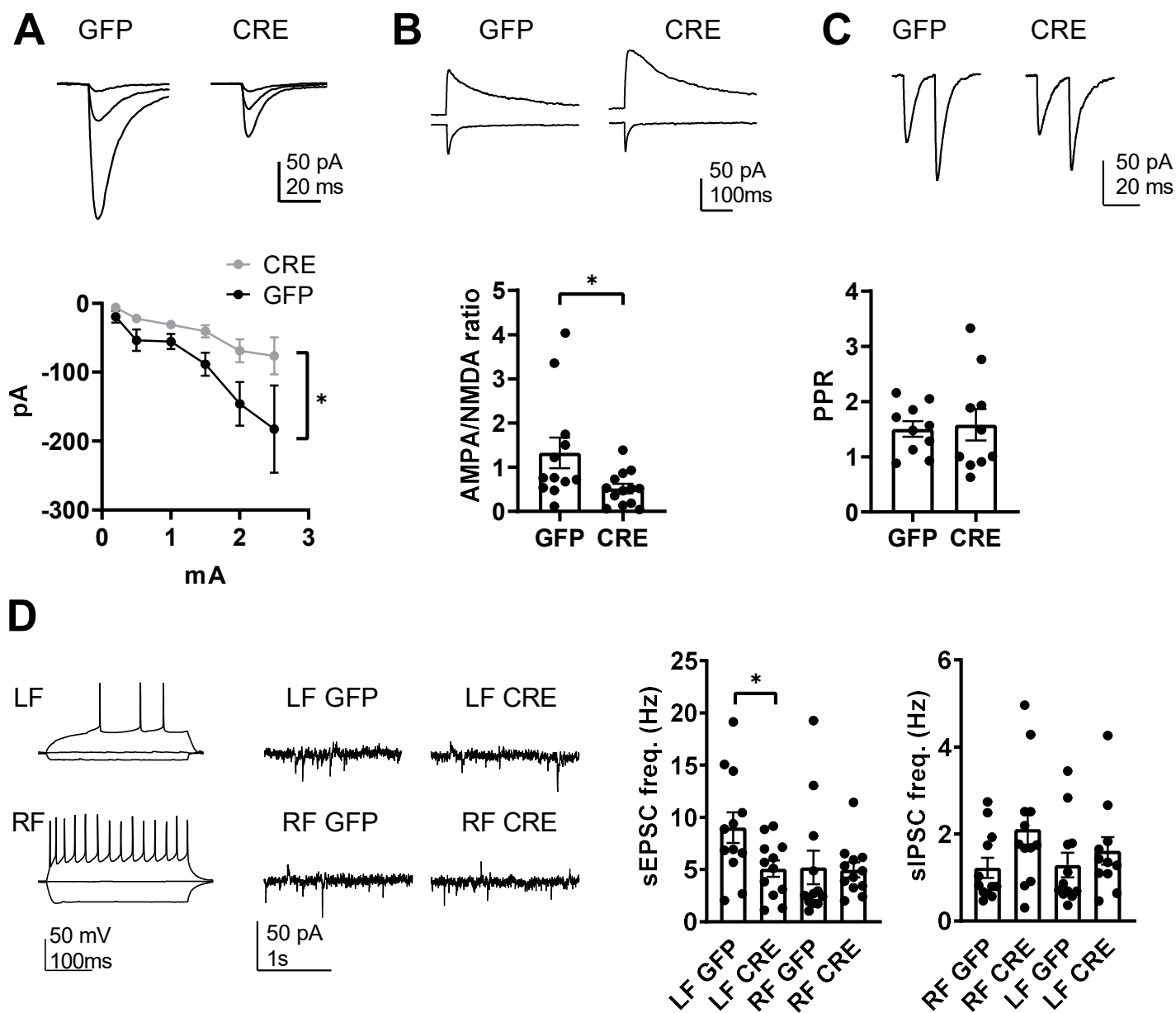


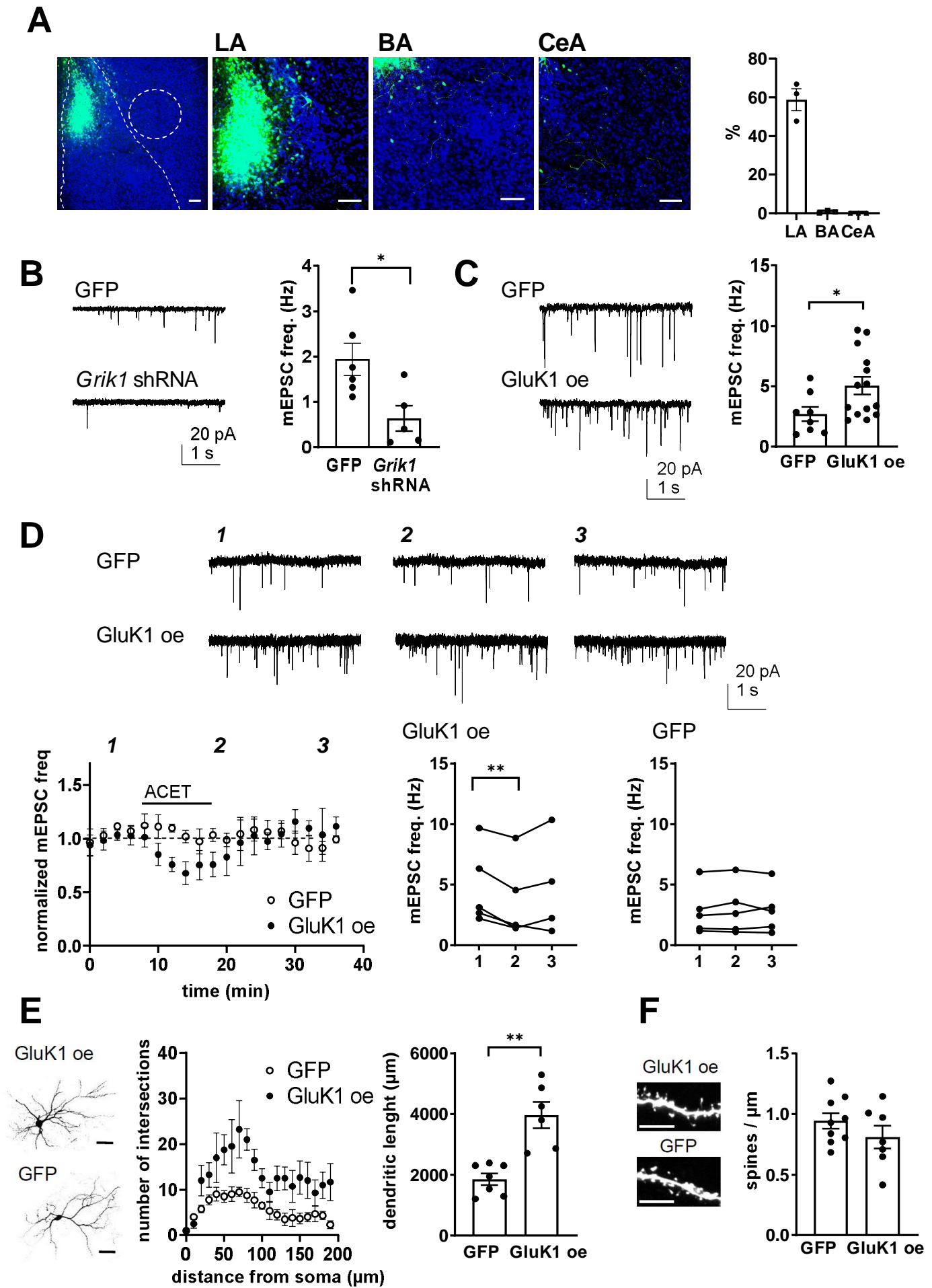
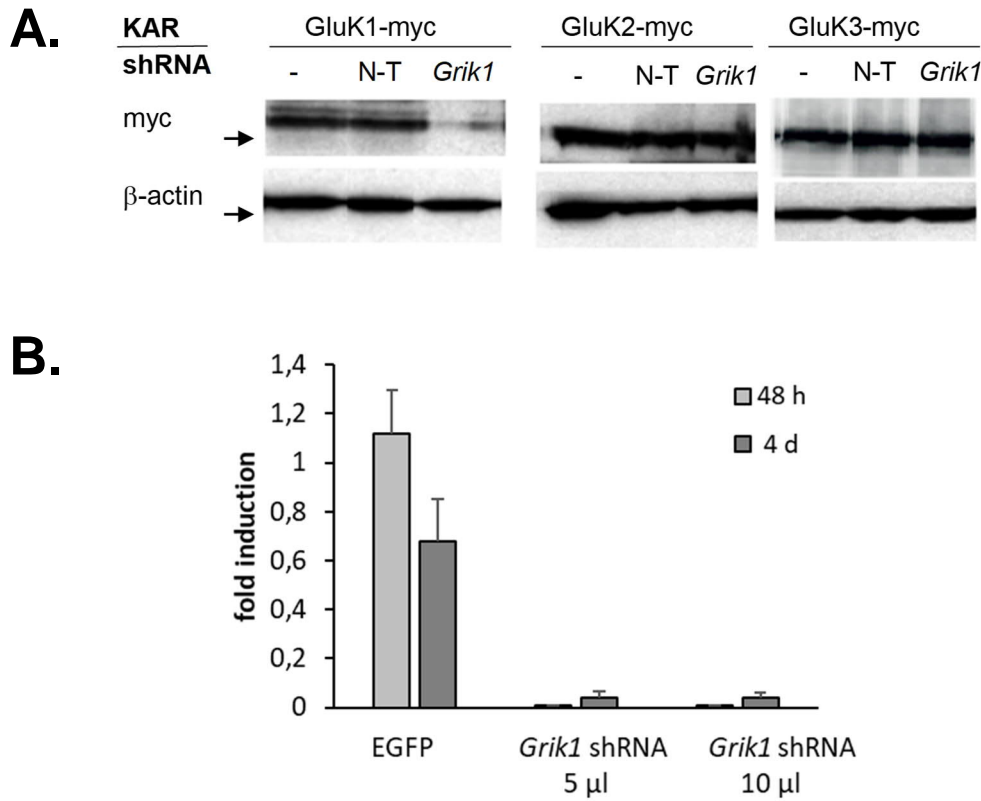
Figure 8

Figure 8 - Supplement 1



Validation of the *Grik1* shRNA

- A western blot illustrating that the *Grik1* shRNA strongly inhibited expression of GluK1-myc but not GluK2-myc or GluK3-myc in HEK293T cells.
- RT-qPCR results showing that the lentiviral *Grik1* shRNA construct strongly inhibited expression of endogenous GluK1 in dorsal root ganglion (DRG) neurons within 48 h from infection.

Methods:

Seven different shRNA sequences against rat *Grik1* in pLKO.1 vector (five obtained from Sigma Aldrich and two from TRC shRNA library, Biomedicum Helsinki Functional Genomics Unit) were tested for their efficiency to suppress expression of GluK1-myc and GluK2-myc and GluK3-myc in HEK293T cells as described (Sakha et al., 2016). The TRC Clone ID: TRCN0000100308 was selected based on its efficiency and specificity to knock down expression of the target protein in the heterologous system. The shRNA target sequence (CCTGGACATTATCAGTCTCAA) was subcloned into a modified pLKO.1 vector where the puromycin resistance cassette was replaced with GFP under the synapsin -1 promoter (pLKO.1-syn1-EGFP). Lentiviral particles were produced in HEK293T cells as described (Vesikansa et al., 2012). The lentiviral *Grik1* shRNA was then further tested in primary dorsal root ganglion neurons (DRG) where GluK1 KAR subunits are endogenously expressed. The neurons were prepared and cultured as described (Kysenius et al. 2012) and infected with the shRNA encoding lentiviral vectors at 4 and 7 DIV. For quantification of the *Grik1* mRNA levels, total RNA

was isolated from two independent cultures at 9 DIV and 12 DIV and RT-qPCR with Grik1 selective primers was carried out essentially as described (Sakha et al., 2016).

References:

Kysenius K, Muggalla P, Mätlik K, Arumäe U, Huttunen HJ. (2012) PCSK9 regulates neuronal apoptosis by adjusting ApoER2 levels and signaling. *Cell Mol Life Sci.* 69(11):1903-16.

Sakha P, Vesikansa A, Orav E, Heikkinen J, Kukko-Lukjanov TK, Shintyapina A, Franssila S, Jokinen V, Huttunen HJ, Lauri SE. (2016) Axonal Kainate Receptors Modulate the Strength of Efferent Connectivity by Regulating Presynaptic Differentiation. *Front Cell Neurosci.* 10:3.

Vesikansa A, Sakha P, Kuja-Panula J, Molchanova S, Rivera C, Huttunen HJ, Rauvala H, Taira T, Lauri SE. (2012) Expression of GluK1c underlies the developmental switch in presynaptic kainate receptor function. *Sci Rep.* 2:310.

Contributions :

Tiina-Kaisa Kukko-Lukjanov, Western blots in HEK cells, lentiviral vectors

Ester Orav, RT-qPCR

Kärt Mätlik , DRG cultures